Title

Modeling Ember Behavior and Accumulation Patterns on and Around Sample Homes During a Wildfire

Authors

Gellerman, Kevin

Chien, Yu-Chien

Publication Date

2023-12-12

UNIVERSITY OF CALIFORNIA,
IRVINE

Modeling Ember Behavior and Accumulation Patterns on and Around Sample Homes During a Wildfire

MAE 294 COMPREHENSIVE EXAM RESEARCH PROJECT

submitted in partial satisfaction of the requirements for the degree of

MASTER OF SCIENCE
in Mechanical and Aerospace Engineering

by

Kevin Gellerman

Research Advisor:
Dr. Yu-Chien (Alice) Chien

ACKNOWLEDGEMENTS

I would first like to express my deepest gratitude to Dr. Yu-Chien Chien because this research report would not have been possible without her guidance and support. I reached out in June 2023 with an existing project in mind and she not only welcomed my work, but welcomed me into the Lasers, Flames, and Aerosols group. She regularly provided feedback and recommendations to sculpt my research efforts and the presentation of my work. As part of the group, I was given the opportunity to regularly present the status of my research to her and other group members. I also gained insight into the fascinating ongoing research of other students in the group. Additionally, Dr. Chien encouraged me to attend the UCI Combustion Institute-Summer School, which turned out to be the most fun, hands-on, and interesting portion of my entire Master's Degree journey.

I would like to extend the utmost thanks to Dr. Tirtha Banerjee from the Civil and Environmental Engineering Department. His elective course on the science and engineering of wildfires is what sparked my interest in the subject. I am fortunate to have had the opportunity to refine and build upon early findings I made in that class to produce this report. He provided great support in crafting the sequence and content of the research.

I am grateful for Dr. Alec Peterson from the Civil and Environmental Engineering Department. As a postdoc in Dr. Tirtha's lab with a focus on field experiments for ember transport dynamics, he was readily available to provide practical research advice.

I'd also like to recognize Dr. Derek Dunn-Rankin for getting me in contact with Dr. Chien and sponsoring these efforts, administratively, when needed. This would not have been possible without coordination.

Thank you to Thunderhead Engineering for providing a free academic trial of PyroSim. Their software is the cornerstone of this report.

Finally, I want to acknowledge the Department of the Air Force for sponsoring my Master's Degree and covering tuition costs for the duration of the program.

Table of Contents

Table of Contents 3
Abstract 4
1. Background 4
2. Methods 7
2.1. Software Validation and Benchmarking 7
2.1.1. Upstream Boundary Layer 8
2.1.2. Flow Around Cube 9
2.1.3. Details of Cube Flow 12
2.2. Building Design 12
2.3. Model Setup and Geometry 14
2.4. Data Visualization and Collection 15
2.5. Variation in Simulation Parameters 15
2.5.1. Ember Size, Density, and Shape 16
2.5.2. Wind Speed 18
2.5.3. Ember Count 20
2.6. Meshing and Rasterization of Angled Objects 21
3. Results 22
3.1. Building Design 22
3.1.1. Roof Ember Accumulation 22
3.1.2. Zone 0 Ember Accumulation 25
3.2. Varying Horizontal Wind Speed 25
3.3. Fire Effects on Benchmark Turbulent Flow 26
3.4. Fire Effects on Ember Accumulation for Model Home 29
3.5. Spatial Temperature Data 31
4. Discussion and Conclusions 33
4.1. Discussion: Highlights, Shortcomings, Future Work 33
4.2. Conclusions 33
5. References 34
6. Appendix 36
6.1. Reference Paper Turbulent Flow Around a Cube 36
6.2. Reference Paper Details of Cube Flow 38
6.3. Model Home Dimensions 39
6.4. Effects of Ember Size and Density - Additional Trials 40
6.5. Effects of Wind Speed - Additional Trials 41
6.6. Visualization of Ember Accumulation 42
6.7. Fire Effects on Benchmark Flow - Additional Plots 44

Abstract

Embers are a potent mechanism for wildfire propagation because the particles can carry farther than the flame front and nullify defensible zones. PyroSim, a Fire Dynamics Simulator (FDS) tool that visually processes text editor inputs for simulating fire-driven fluid flow, is leveraged to model ember transport and accumulation patterns on buildings during a wildfire. This research begins with benchmark analysis against existing findings in literature for validating its usage. It focuses particularly on the transport and accumulation patterns of non-combusting particles with realistic ember parameters which are carried via wind over sample buildings. This study tested various ember sizes, ember densities, wind speed in the horizontal and vertical direction, rooftop styles, and fire effects to examine how each factor impacted ember behavior. Results indicate that roofs with a ridge line perpendicular to wind direction are more likely to accumulate embers. Additionally, horizontal and vertical wind speeds must be strong to facilitate ember transport but not so great that embers are unable to deposit and settle onto buildings. Regardless of building design, a plurality of embers come to rest against the front-facing walls of the structure, posing the biggest risk to fire spread. Surface fires impact flow behavior, so a ground fire was introduced to the model to examine how results change. Ultimately, it is theorized that fire-driven turbulence may facilitate ember transport but negate accumulation in unstable regions, such as rooftops.

1. Background

Wildfires can spread through direct flame contact, radiant heat transfer, or spotting of firebrands. Embers, or firebrands, form as a fuel structure degrades into smaller particles, and these particles can be lofted upward by the fire plume where they become captured by wind. Embers are a particularly potent mechanism for wildfire propagation because the wind-driven particles can carry farther and faster than the actual flame front [1].

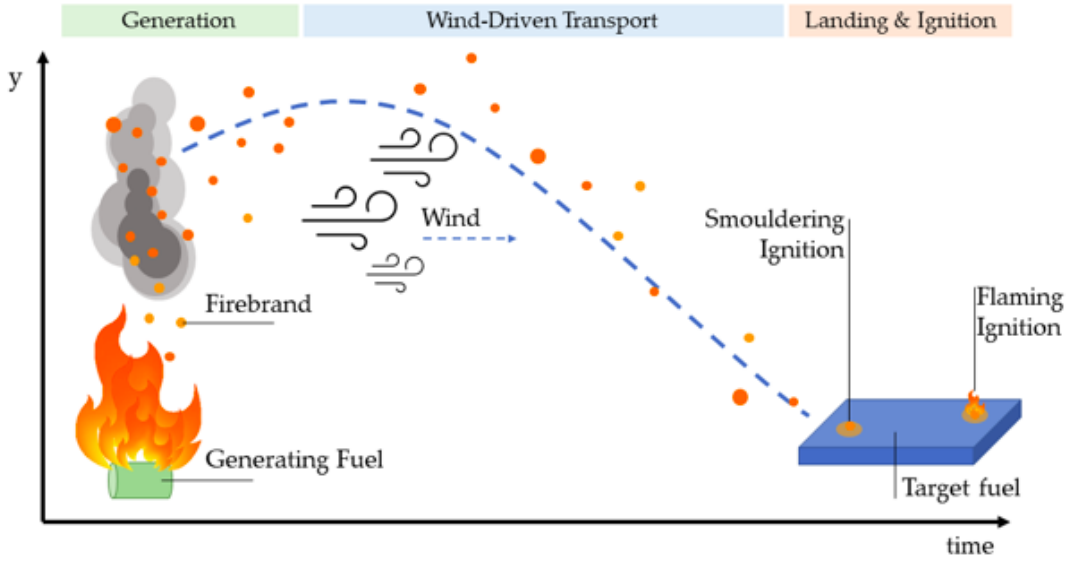

Figure 1: Firebrand Spotting Diagram [1]

Fire lawmakers have coined the term “Home Ignition Zones” to define Defensible Space Zones around residential buildings to minimize damage to homes during wildfires. Zone 1 is the “Lean, Clean, and Green” zone and it spans the region 0 - 30 ft (~0 - 9 m) from the home. Zone 1 should be completely free of major combustibles. Zone 2 is the “Reduced Fuel Zone” and it spans the region 30 - 100 ft (~9 - 30 m) from the home. Zone 2 outlines requirements for allowed vegetation height, distance between flammable objects, and build-up of fallen debris. However, fire experts point to the importance of Zone 0, or the “Ember Resistant Zone” which spans 0 - 5 ft (~0 - 1.5 m) but is not required by law. Despite this, it has been cited as the most important defensible space because it prevents fire from spreading directly to the home. In Zone 0, landscaping, outdoor furniture, and debris should all be carefully maintained and selected to remove all combustibles [2,3]. These defensible zones will inform the model dimensions and data collection for much of the findings in this report. This research covers regions from all zones, but contains more detailed analysis on Zones 0 and 1.

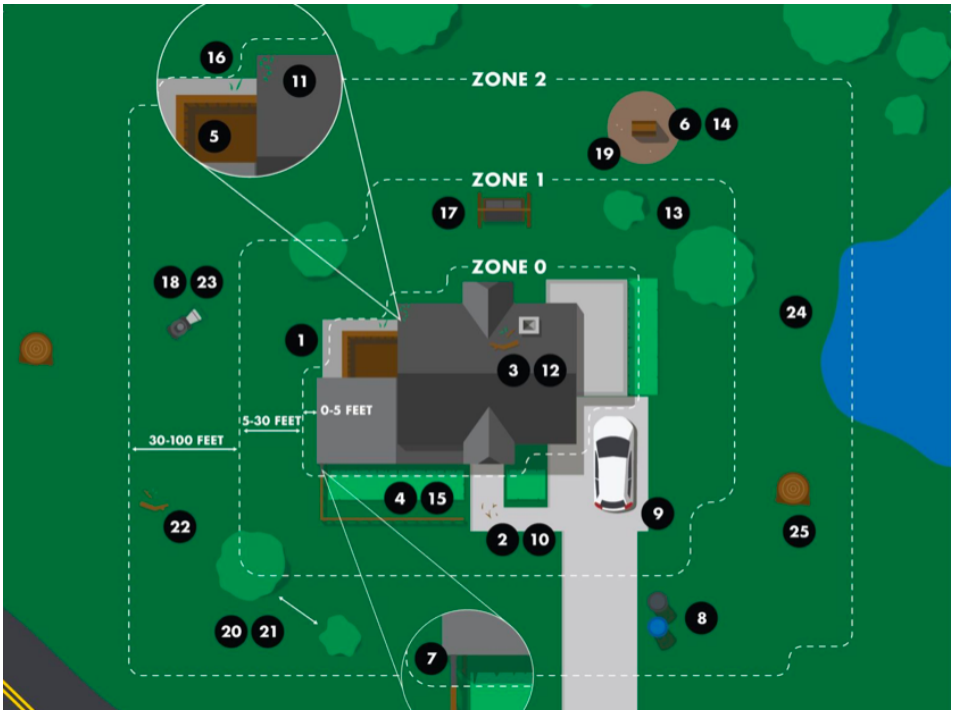

Figure 2: Defensible Zones [2]

Research into the behavior and accumulation of embers on buildings, such as those in Wildland Urban Interfaces (WUIs), is limited. The Institute for Business and Home Safety (IBHS) has experimented with the effects of an ember storm on a full-scale sample home. They assessed how the building and its surroundings readily ignited in regions with available target fuel. The study produced some general observations regarding firebrand accumulation near rough and smooth surfaces along with general building features such as vents, fences, and decks. It also determined firebrand accumulation rates in water pans adjacent to the building, but failed to examine accumulation rates on the building itself [4].

One study set out to quantify how embers accumulate on the rooftops of isolated buildings during an ember storm. To do so, they conducted several scaled-down wind tunnel experiments on a variety of rooftops at different wind speeds and angles using blended pine straw to mimic embers. In this report, the sample building designs roughly resemble the basic shapes used in the wind tunnel study. The authors found that very little of the ember introduced into the system came to rest on the roofs, but those that did accumulate along internal corners. Buildings without these corners had negligible accumulation and were not reported. Finally, they point out that as wind speed increases, accumulation rates decrease, likely because the streamlines around buildings become more difficult to cross [5].

Another study conducted simulations on ember accumulation for a sample WUI home using PyroSim [6]. In this study, wind speed, the friction factor of the building, and the mass flux of embers introduced into the system were all varied. In line with the last study cited, accumulation decreases at greater wind speeds. As expected, accumulation rates were directly

proportional to the mass of embers introduced to the system. Importantly, the study found that friction has a limited effect on accumulation rates due to limitations in the FDS/PyroSim software.

This research analyzes ember accumulation for various building layouts and roof designs. This work will initiate the simulation in a manner similar to that of work [6] and apply semi-realistic ember parameters to an ember storm over a variety of structure shapes to determine what simple design factors contribute to ember accumulation. The detailed methods and phenomenon will be addressed and discussed in the Methods Section of this report.

Finally, PyroSim is an add-on to Fire Dynamics Simulator (FDS) developed by Thunderhead Engineering. FDS is a large-eddy computational fluid dynamics (CFD) software model that predicts turbulent fire-driven fluid flow by solving time-dependent, three-dimensional flow fields using the Navier-Stokes equations. Typically FDS reads input parameters from a text file and outputs a numerical solution, but PyroSim offers a graphical interface that generates input parameters to FDS for the user [7].

2. Methods

2.1. Software Validation and Benchmarking

Before performing simulations relevant to this report's findings, PyroSim LES calculations were valid. To begin we considered a very simple case of horizontal wind flow over a bluff body approximately on the scale of real-world buildings. Here, an inlet is defined that allows air to flow into a system at 5 m/s. The air then passes over a 5m x 5m x 3m cube that disrupts streamline flow. As a proof of concept, mock air particles are tracked over time to confirm that the bluff body breaks up the streamline flow and forces air to travel around the building while simultaneously introducing vorticities along the tail edge. Turbulent flow is dominated by vortex dynamics, or the circular motion of fluid, and as such, their presence is a tell-tale sign of turbulent flow [8]. This behavior is confirmed by simple observation of the air particle trails traveling in the negative x direction (right to left) in Figure 3, below.

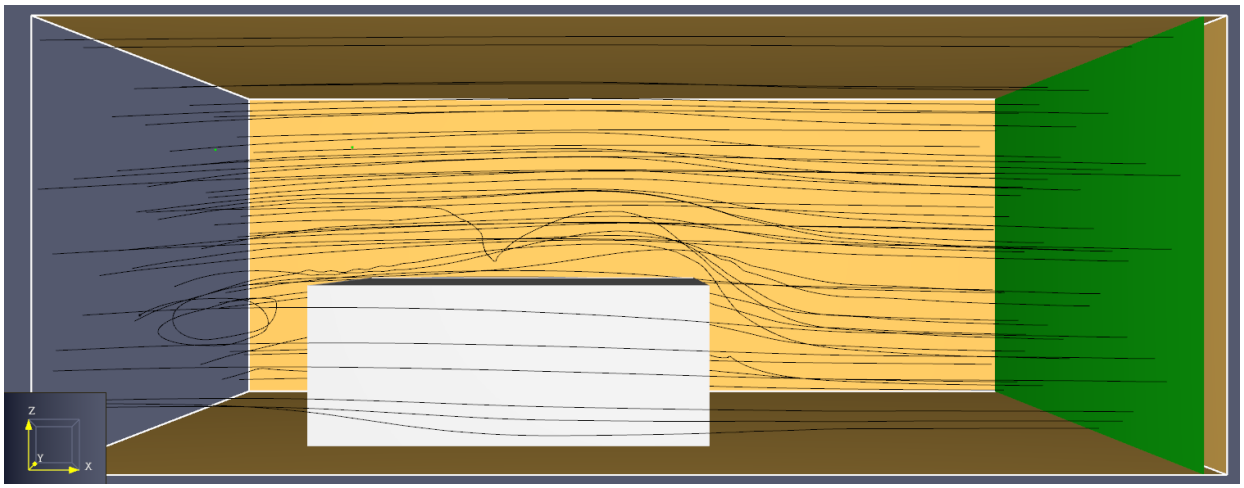

Figure 3: Air Particle Trails over Bluff Body 5m x 5m x 3m at 5 m/s

With the simple confirmation of turbulent behavior complete, the results of PyroSim were then systematically and scientifically validated and benchmarked against a paper by Lim et al. studying LES bluff body flow around a cube in a turbulent boundary layer [9]. Here, we replicate the procedures from the paper and design a mock wind tunnel with a small cube at its center. The cube has a side length of 0.1 m, denoted by the variable h. The wind tunnel has a domain of 6h x 3h x 2h and a grid size of h/20, or 0.005 m. The domain is sufficient to create steady, free-stream flow before, after, and around the cube. The mesh resolution is sufficiently fine to capture all complex features of flow around the cube quite well. Free-slip boundary conditions and surface roughness conditions were chosen to match those in the paper for ideal comparison. Again to match the paper, calculations were carried out at a Reynold's number of 20000 and a corresponding free stream velocity of 2.96 m/s in the negative x direction. The trials ran over 5 seconds with a 1-second ramp-up time for velocity. All results contain time-averaged data from 2.5 to 5 seconds to measure fully developed turbulent flow over many

time-steps. Raw temporal velocity data at each grid point was exported from PyroSim and uploaded to MATLAB for post-processing and visualization.

2.1.1. Upstream Boundary Layer

First, we examine the approaching turbulent boundary layer to confirm that the velocity profile is as expected. Here, we take the horizontal component of velocity along a vertical centerline of the domain upstream of the cube before flow is perturbed. This data is taken 0.25 m downstream from the inlet of the domain which is the start of the boundary layer. Primarily, we intend to verify whether the boundary layer thickness matches theoretical calculations and whether or not it obeys linear log-law behavior within the boundary layer region. To calculate theoretical boundary layer thickness, we consider the approximate equation for turbulent boundary layers along a flat channel plate [10].

$$\delta(x) \approx 0.37 \frac{x}{Re_x^{1/5}} \quad (1)$$

Taking the distance from the start of the boundary layer (x) to be 0.25 m and Reynold's number (Re) to be 20000, we calculate a boundary layer thickness of approximately 0.0128 m. This is the distance at which the velocity profile essentially reaches freestream velocity. In the simulations, the velocity profile near the boundary reaches the free stream flow at approximately 0.015 m, so the findings are congruent, considering the grid size. When plotted on a log scale, the velocity profile is relatively linear inside the boundary layer. Therefore, these results are considered reasonable with the magnitude and trend shown in Figure 4.

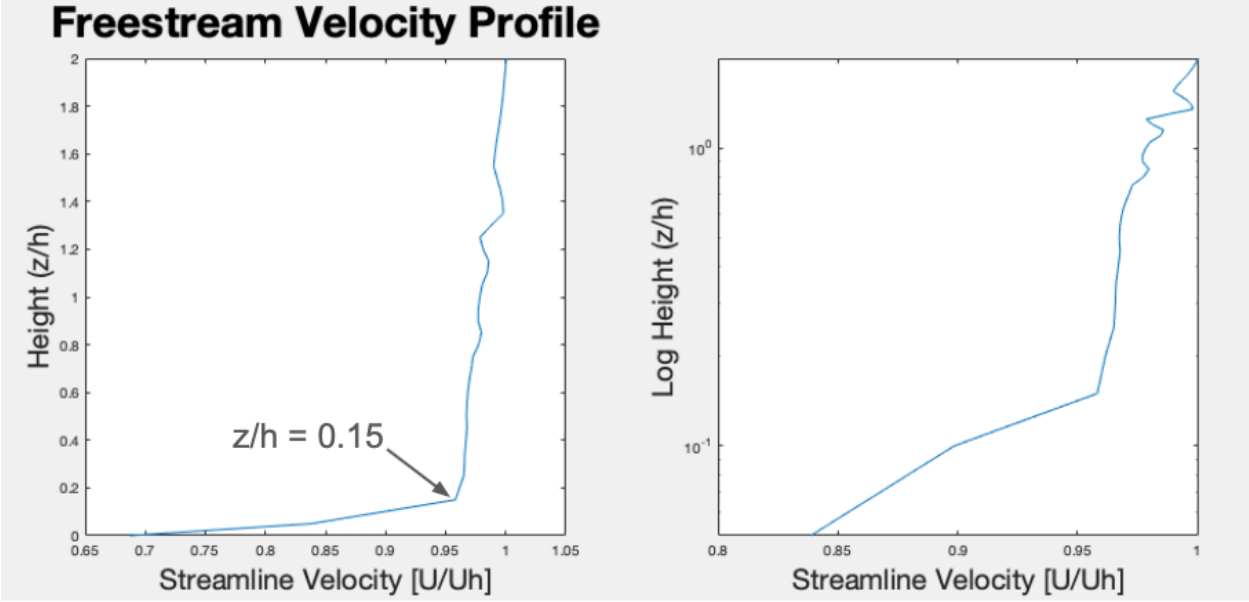

Figure 4: Upstream Velocity Profile

2.1.2. Flow Around Cube

Next, the results for the overall flow around the cube are examined. The mean velocity vector field and vorticity fields are considered with axis values normalized by the size of the cube h. First of all, we examine flow behavior in the x-z plane. The (u,w) velocity vectors corresponding to the x-z plane are displayed in Figure 5. The mean vorticity contours of the y-component of vorticity (ω_y) are displayed in Figure 6. Note that the vorticity of a velocity field is defined to be the curl of the velocity field. In component form, vorticity is calculated as follows [11].

$$\omega = \left(\frac{dw}{dy} - \frac{dv}{dz}, \frac{du}{dz} - \frac{dw}{dx}, \frac{dv}{dx} - \frac{du}{dy}\right) \quad (2)$$

On the ground, just upstream of the cube, a small recirculation pattern can be observed. Above this region, there is a stagnation point on the front face of the cube. Over the top of the cube, there are signs of a separation region and a downstream wake can be identified as well. These results and flow patterns align with the findings of Lim et al. well. Note that the vorticity directly upstream of the cube is not entirely resolved, but it is bouncing around zero, which is what the value should be.

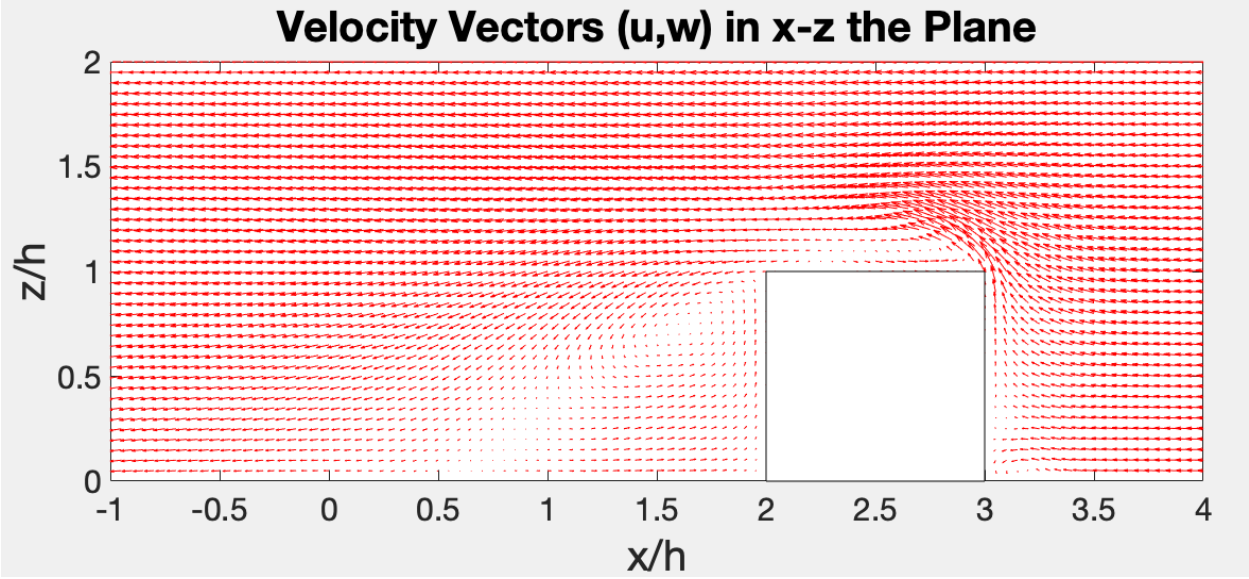

Figure 5: Velocity Vector field in the x-z Plane

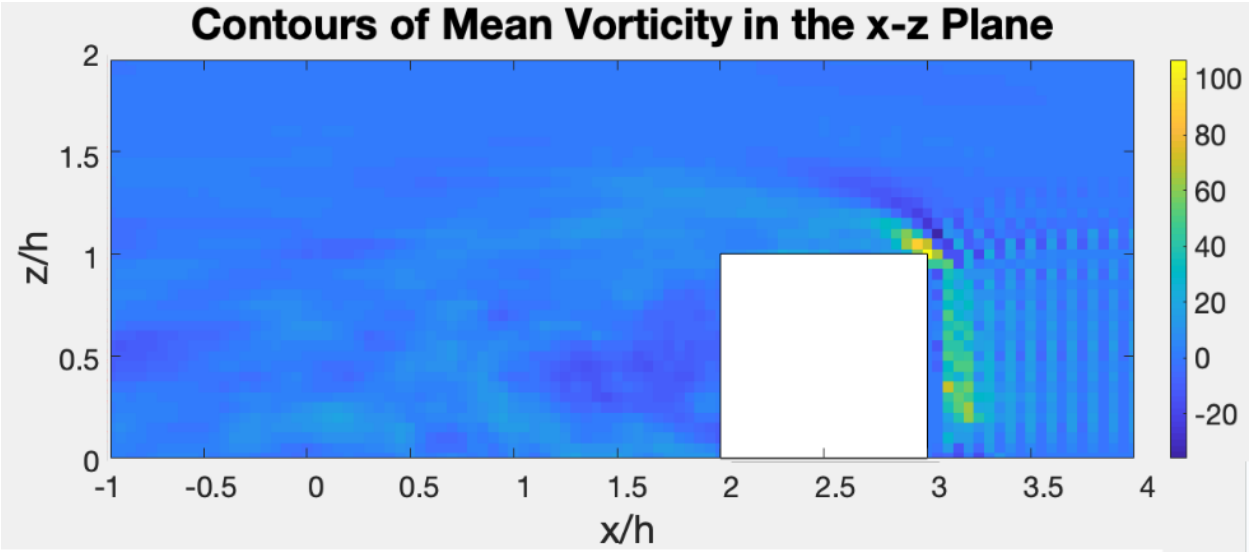

Figure 6: Contours of Mean Vorticity (ω_y) in the x-z Plane

Secondly, we consider crosstream flow behavior in the y-z plane. The (v,w) velocity vectors corresponding to the y-z plane are displayed in Figure 7. The mean vorticity contours for the x-component of vorticity (ω_x) are displayed in Figure 8. There are signs of strong convergence in the region directly surrounding the cube. The vector field matches very well with the reference paper by Lim et al, but the vorticity contours do differ slightly. Despite this, positive and negative regions of vorticity match the literature, and the contour is as one would expect for the given velocity field, so the results can be considered accurate.

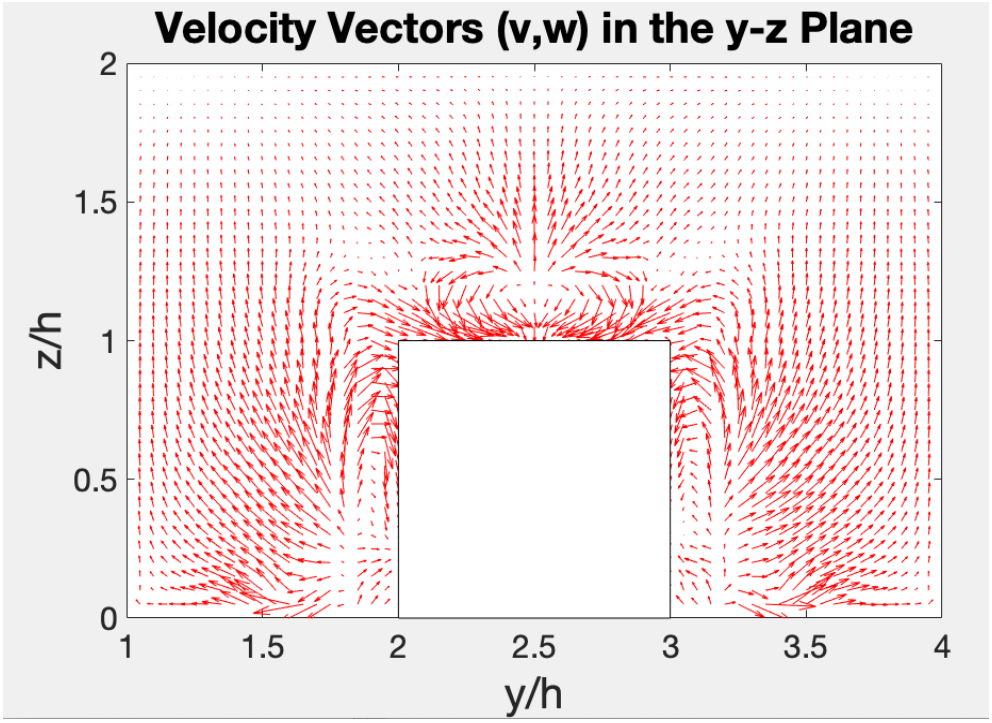

Figure 7: Velocity Vector field in the y-z Plane

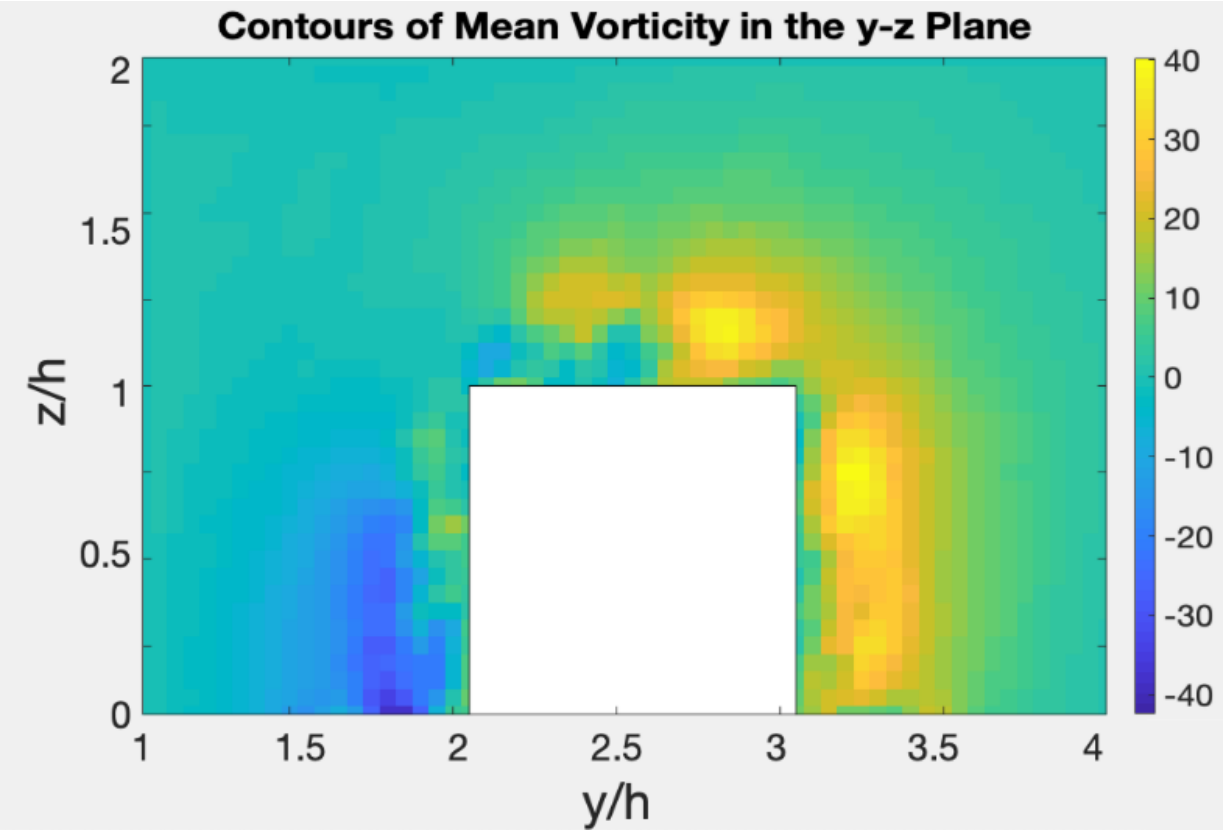

Figure 8: Contours of Mean Vorticity (ω_x) in the y-z Plane

2.1.3. Details of Cube Flow

As conducted in the study by Lim et al., the vertical velocity profiles of mean velocity along the axial centerline of the cube are also plotted. Figure 9 displays the horizontal velocity and Figure 10 displays the vertical velocity along the centerline. Vertical grid lines are equally spaced along the length of the cube to represent how wind flow spatially grows over the cube. The horizontal velocity profiles are similar to the findings of the reference paper. The vertical velocity profiles also align well. One anomaly is the reduced vertical velocity at the surface of the leading edge. The differences can likely be attributed to the no-slip boundary condition applied to the cube in this report, which may differ from the cube's unique surface conditions utilized in the paper. The findings, particularly Figure 10, display an expected flow separation as the boundary layer detaches from the surface into the wake.

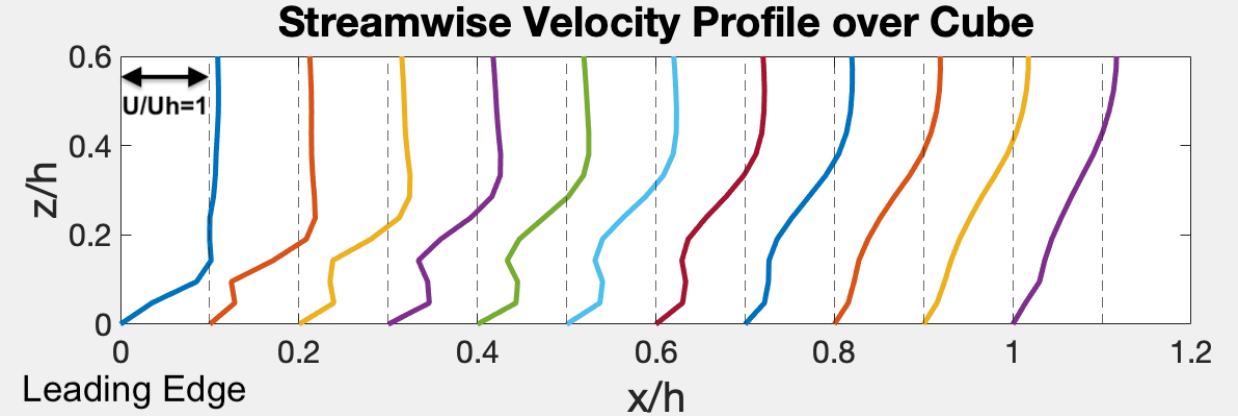

Figure 9: Streamwise Velocity Profiles over Cube

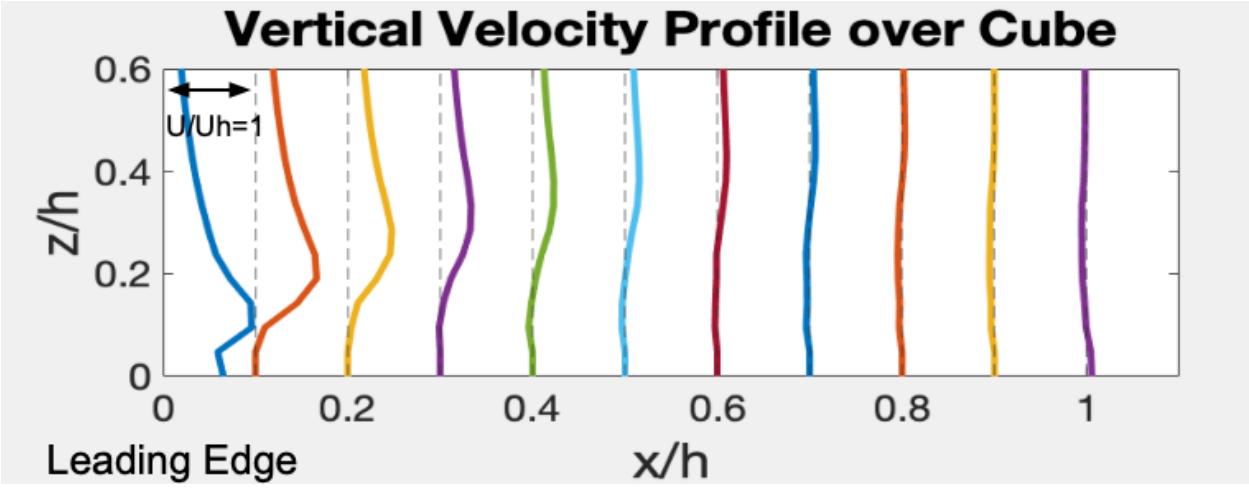

Figure 10: Vertical Velocity Profiles along Cube

2.2. Building Design

Next, we move on to preparations for simulating ember accumulation on and near residential buildings. Google SketchUp was used to build five basic house structures. These include square, rectangular, L-Shaped, T-Shaped, and IBHS replica buildings. Several of the designs were pulled from the wind tunnel experiments conducted by Nguyen et al. [5]. Each building was designed to fit within a 10 x 10 m box with the longest edge spanning exactly 10 m. This was done to ensure consistency of size across each building along with a size that applies to the scale of real-world WUI structures and homes. For consistency, each building has a 3 m ceiling height, which is similar to the average ceiling height in the United States of 8 to 9 ft [12]. Additionally, for consistency of slope, all roofs were designed with a common 6:12 pitch, meaning that vertical height increases in relation to horizontal distance by a proportion of one-half [13]. This ensures steeper or more shallow slopes do not influence accumulation across building shapes. The IBHS model is not an exact replica, but rather an estimation based on images of the full-scale home used during ember storm tests. The models, pictured below, were downloaded

from SketchUp as Drawing Exchange Format (.dxf) files and imported into PyroSim as a 3D geometry. Dimensions are given in Section 6.3 of the references.

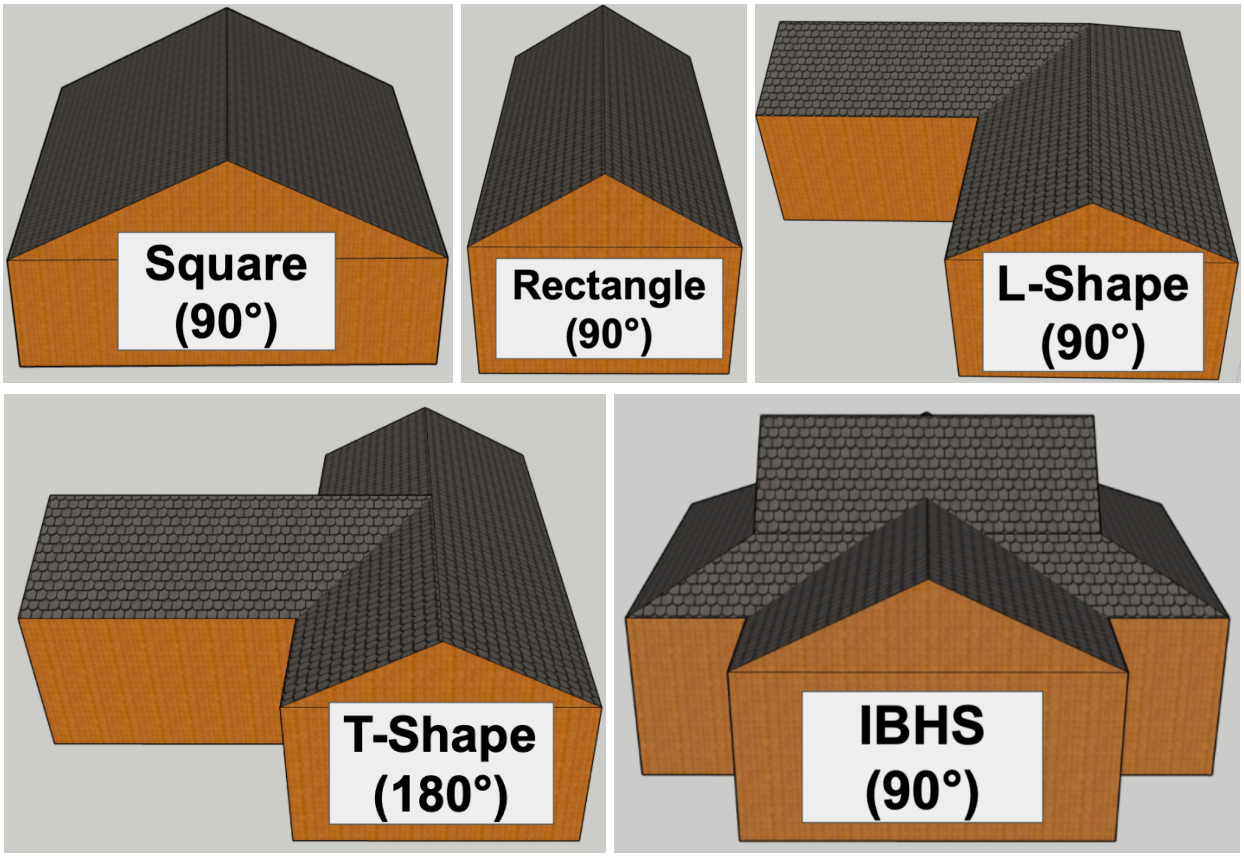

Figure 11: Square, Rectangular, L-Shape, T-Shape, IBHS Replica House Models

Note that each of these pictures is identified as the 90° or 180° configurations. The houses are non-symmetric and trials need to be run for each house at different angles relative to the horizontal wind direction. Also note that the convention for Figures in this paper is wind flowing in the negative x direction from right to left. For each of the configurations illustrated, the dominant ridgeline is perpendicular to that wind flow.

2.3. Model Setup and Geometry

The simulation is confined to a rectangular prism with a domain of 30 x 30 x 10 m. The 10 x 10 m house plot begins 10 m from an “Inlet” vent that can introduce wind, mass, or heat to the system in the negative x direction. This distance was selected because it is roughly equal to Defensible Space Zone 1, described in the Background section, which covers 30 ft from the edge of a home [2]. Zone 1 acts as a buffer for approaching wildfires and ordnance dictates that there should be limited vegetation or other fuel sources that would lead to fire propagation in this region. As such, this distance is critical to ember carry as the fire can spread to fuel sources present in Zone 1 and create embers that deposit past 10 m downwind at the house. The 10 x 10 m plot ends 10 m before the “Outlet” vent. This space allows the simulation to track embers

in the turbulent wake of the home where they may recirculate. The Outlet acts as an exhaust that is exposed to ambient conditions and ensures mass is not forced to accumulate inside the bounds of the system.

Next an “Ember Cloud” that generates particles or embers is constructed. Behind the ember cloud is a “Blower” which allows one to specify horizontal and vertical wind speeds that the embers are subject to. The Ember Cloud and Blower are 3 to 5 meters above the ground and span the depth of the domain. This is done to facilitate ember transport and ensure that a majority of the embers land in the house plot to achieve high ember flux concentrations while limiting the total number of embers for computational speed. Each simulation described in this report spans a 30-second window. During the first 5 seconds, no embers are injected as the Inlet wind ramps up to full speed. For the next 20 seconds, embers are actively injected into the system from the ember cloud according to the rate described in Section 2.5.2, below. During the final 5 seconds, ember injection is halted. During this time the wind remains unchanged as embers already in the system are given time to deposit and settle or exit the system.

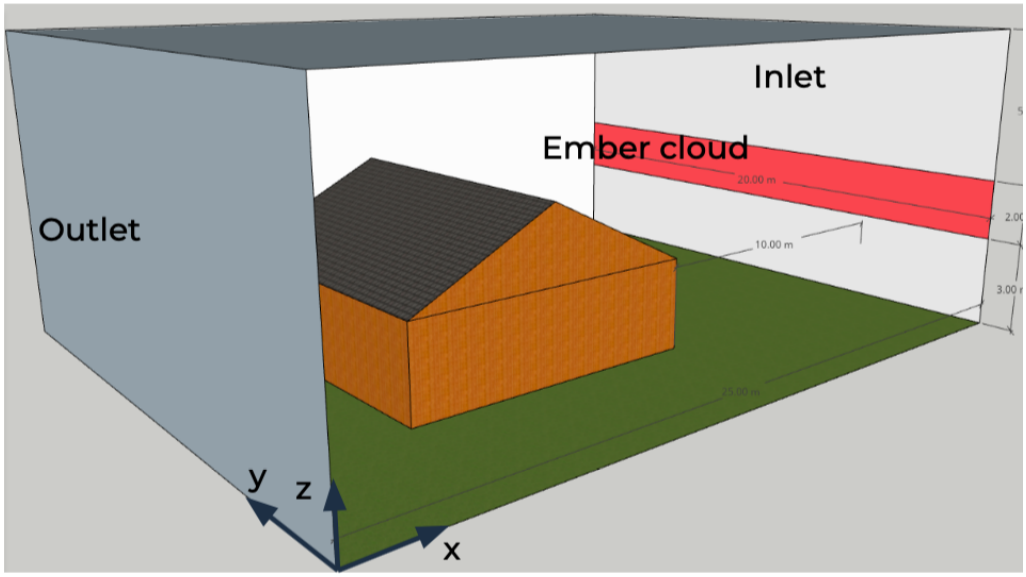

Figure 12: Model Geometry (90° Square Home)

2.4. Data Visualization and Collection

To visualize the concentration of embers, PyroSim’s “Plot3D” Output menu was used. The mass per unit volume of the ember particles was selected as the outcome to be visualized. To measure the numerical mass of accumulated embers, a “Gas Phase Device” was created. Here coordinates are provided to generate a bound around the roof of each building and another around defensible Zone 0 extending ~1.5 m out from each wall at ground level. PyroSim then determines the total volume of embers within a domain and takes a volume integral to achieve total mass as a singular output. To ensure this system produces accurate results, one must manually calculate the total mass of ember particles entering the system per unit time and provide that value as an input. This is very simply found by calculating the volume of each

particle and multiplying by density to obtain the mass of a single ember. PyroSim uses the mass per unit time input along with the ember count to reverse engineer ember parameters not listed as inputs to the system.

Ultimately, Plot3D outputs a visualization of mass per unit volume with areas containing many embers highlighted as critical accumulation zones. The Gas Phase Device outputs a .csv file that shows the total mass of embers within each specified domain as a function of time.

2.5. Variation in Simulation Parameters

Before simulating ember behavior and accumulation patterns during a wildfire, we need to determine ember size, density, shape, and wind conditions as input parameters. The goal is to select values that simulate realistic ember storm characteristics defined in the literature. Simultaneously, we must facilitate ember travel and accumulation in distances relevant to the defensible space zones construct described in the Background section.

2.5.1. Ember Size, Density, and Shape

Typically, embers are modeled as having spherical, cylindrical, or disc shape. Due to limitations in PyroSim's ability to handle complex moments of inertia and non-uniform drag, all particles are calculated as spheres, regardless of the data input for the geometric dimensions of the particle. To examine how variations in size or density affected ember behavior, we defined six regions within the area of the model domain, described above, that capture embers with a back wall. The walls encompassing each region have a height of just 1 m so as not to interfere with flow. Each region occupies a space of 6 m in the x direction and the full 30 m in the y direction. A Gas Phase System is created to output total mass accumulation in each region. See Figures 13 and 14, below, for a visual of how the regions are defined and an example of embers (pictured as red dots) being trapped in the regions at the close of a simulation. Note that regions 2, 3, and 4, which occupy the space 6 - 24 m from the inlet are of particular interest because the model homes fall within this space.

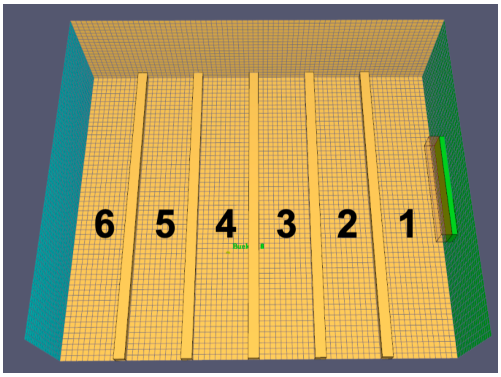

Figure 13: Ember Collection Regions

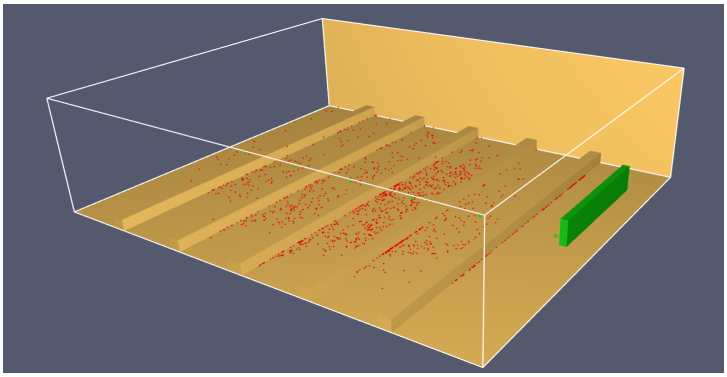

Figure 14: Ember Collection Example

By observation, embers that would have otherwise deposited in one region would occasionally hit the back wall and get lifted upwards to get carried further than their initial deposition site. This occurrence was rare but should be noted. Additionally, refining the mesh resolved turbulent flow behavior and slightly altered results. As such, plots in this section contain a modest 10% error bar to account for these observations. Early trials were performed with a coarse mesh of just 40,000 nodes. Select trials were repeated with a refined mesh of 400,000 for accuracy. Plots for the ember distribution and Tables containing the percentage of embers exiting the system are included below. To reduce clutter, the course mesh trials with additional data points are included in Section 6.4 of the Appendix.

To begin, we tested several different ember sizes to examine how varying radius affects carry distance. Here, density, horizontal wind speed, and vertical wind speed are held constant at values of 60 kg/m^3, 5 m/s, and 3 m/s, respectively.

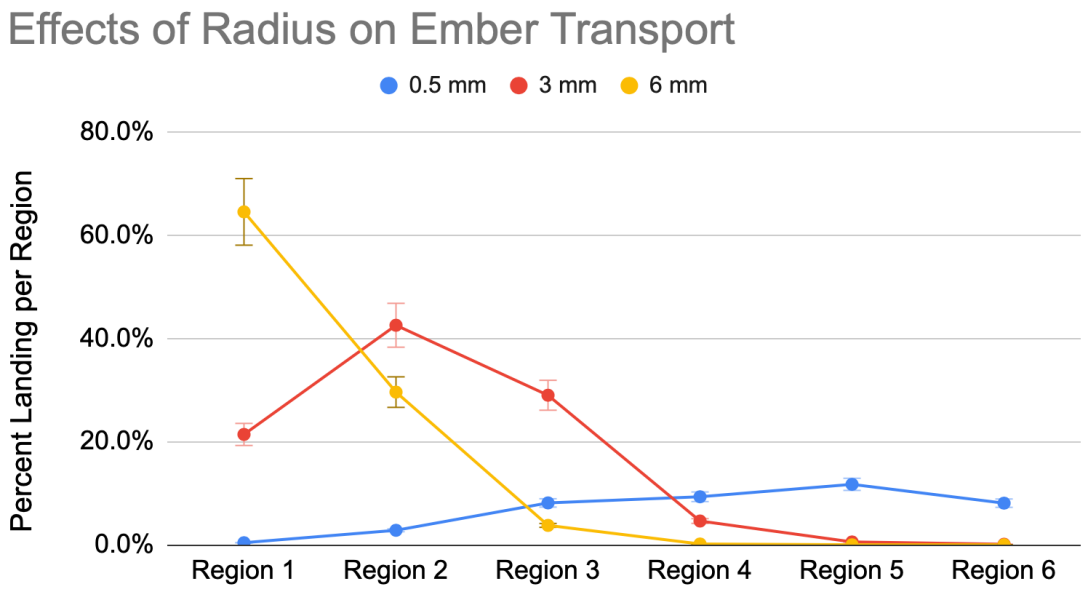

Figure 15: Effects of Ember Radius on Transport

Table 1: Ember Size - Percent of Embers Exiting System

Radius [mm]	0.5	3	6
Embers Exiting System [%]	59.7	1.9	2.1

As expected, larger embers do not travel as far due to their increased mass. For all future simulations, we choose to model embers as 3 mm radius spheres because it maximizes ember count in the regions of interest. This is on the lower end of what has been observed in most studies, but it is present in literature [14]. The smaller size helps reduce total weight and facilitates the transport of the embers via wind. Next, we test several different ember densities. Here, ember radius, horizontal wind speed, and vertical wind speed are held constant at values of 3 mm, 5 m/s, and 3 m/s, respectively,

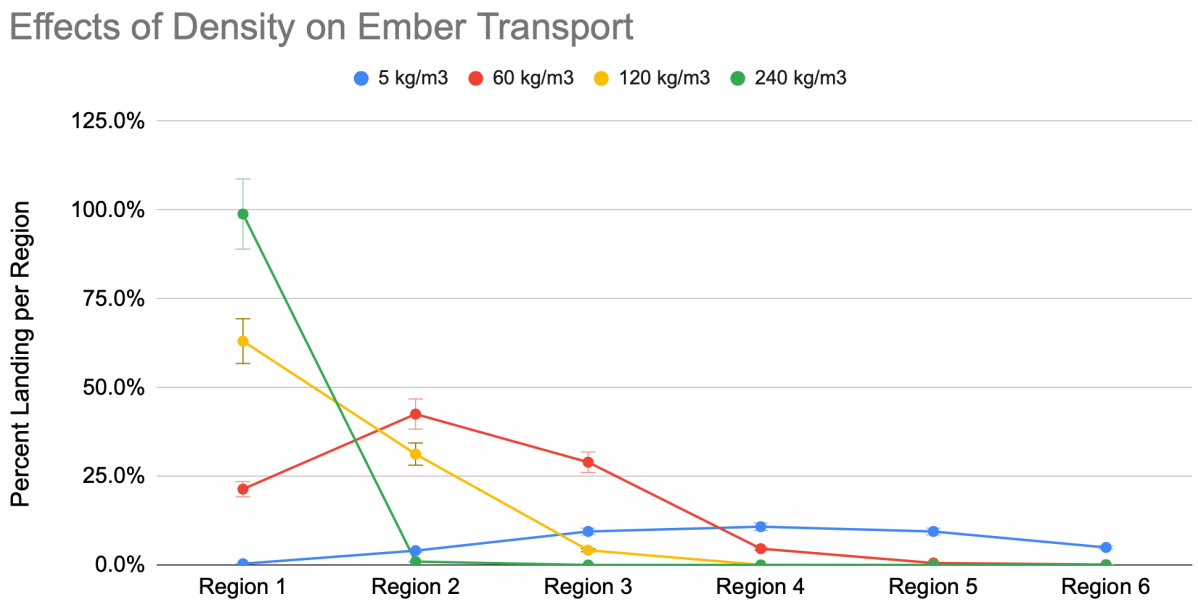

Figure 16: Effects of Ember Density on Transport

Table 2: Ember Density - Percent of Embers Exiting System

Density [kg/m^3]	5	60	120	240
Embers Exiting System [%]	61.0	1.9	1.5	0

As expected, higher density embers do not travel far due to their increased mass. For future simulations, the ember density is selected to be 60 kg/m^3. This, again, is on the lower end of the typical spectrum, but one study measured 60 kg/m^3 as the density for embers generated by Oriented Strand Boards, which is a cheap material made by compressing large flakes of wood together [15]. Again, this low value was selected to assist in ember transportation as higher densities tend to receive little loft, especially at low wind speeds.

2.5.2. Wind Speed

First, we consider several different horizontal wind speeds. Here, ember radius, ember density, and vertical wind speed are held constant at values of 3 mm, 60 kg/m^3, and 3 m/s, respectively,

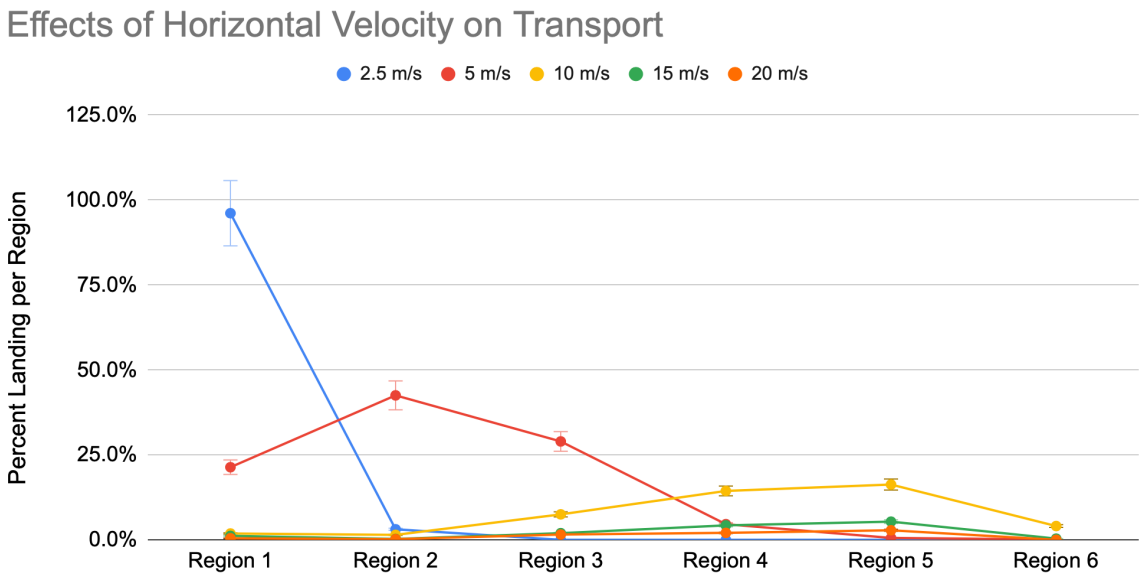

Figure 17: Effects of Horizontal Wind Speed on Transport

Table 3: Horizontal Wind Speed - Percent of Embers Exiting System

Horizontal Wind [m/s]	2.5	5	10	15	20
Embers Exiting System [%]	0	1.9	54.5	86.7	93.0

As expected, higher horizontal wind speed is directly related to ember carry distance. Unless otherwise stated, in future simulations, a velocity of 5 m/s will be selected. It maximizes ember retention in the regions of interest while still creating some loft. Additionally, in literature, it has been noted as the average speed associated with Santa Ana winds during large fire propagations in Southern California [16]. Finally, we test several different vertical wind speeds. During these trials, ember radius, ember density, and horizontal wind speed are held constant at values of 3 mm, 60 kg/m^3, and 5 m/s, respectively.

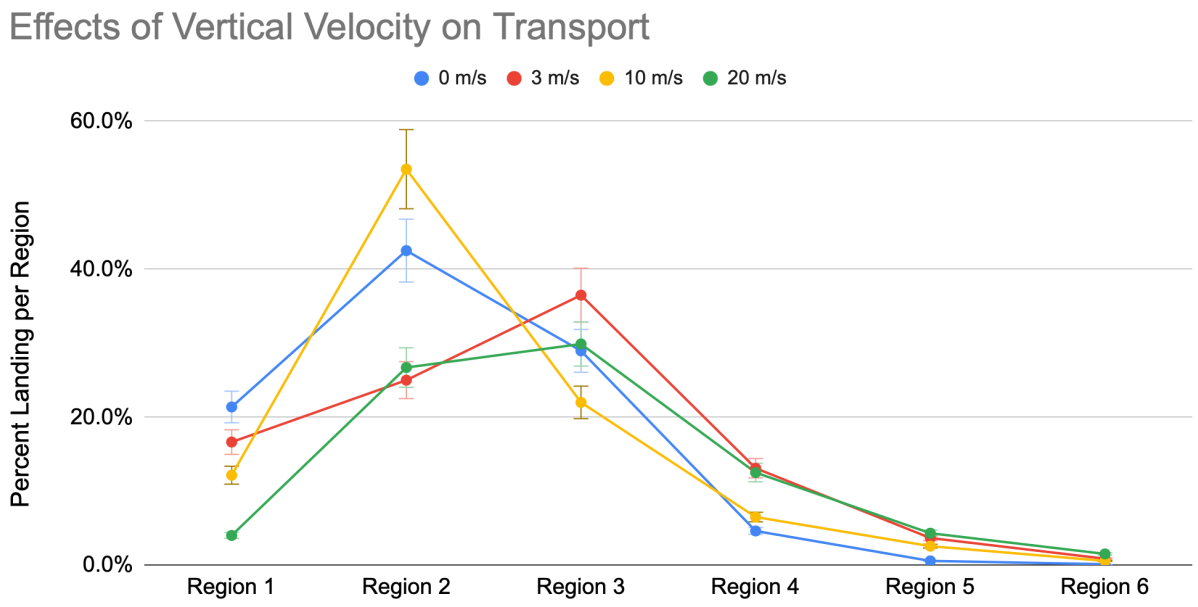

Figure 18: Effects of Vertical Wind Speed on Transport

Table 4: Vertical Wind Speed - Percent of Embers Exiting System

Density [kg/m^3]	0	3	10	20
Embers Exiting System [%]	1.9	4.3	2.8	21.2

The results here are less clear than the others. However, increased vertical wind speed tends towards greater ember transport distance. Unless otherwise stated, a modest vertical wind speed of 3 m/s is selected for all future trials because it does the job of carrying embers to the regions of interest and is not so great that it diminishes realism. It also replicates the vertical loft of a fire plume and introduces some level of artificial turbulence at the inlet of the system. Dr. Alec Petersen, a member of the UCI Banerjee Lab, studies ember transport dynamics in the field and proposed this vertical velocity selection.

2.5.3. Ember Count

The goal is to introduce embers into the system at a rate comparable to real-world wildfires. One paper characterized ember concentrations during an experimental field fire in a pine-dominated environment using many water pans for collection and found fluxes of approximately 0.82 - 1.36 pcs m^{-2}s^{-1} [17]. A later paper analyzed these results and pointed out that the data was heavily influenced by periods of very little ember accumulation. They removed bias from periods of low ember activity and found that flux could reach as high as 7 pcs m^{-2}s^{-1} [18].

To estimate ember flux in the regions of interest, a small wall was created around the 10 x 10 m plot to be occupied by model homes. Next, the ember count injected into the system was systematically varied until that region contained an ember flux matching that in literature. The Gas Phase Device in that region tells us the total mass, and thus the mass per unit time is easily found. Since the mass of an individual ember particle is known, one simply divides the total mass per unit time by the mass of a single particle to find the number of particles entering the critical zone per unit time. Finally, that zone has an area of 100 m^2, so the embers per unit time per unit area is calculated. Ultimately, when the ember cloud injects 800 particles per second over the 20-second simulation duration, the house plot is subject to an ember flux of 1.15 pcs $m^{-2}s^{-1}$, which falls within the bounds of the first citation on ember fluxes during field fires. This indicates that approximately 14.3% of embers entering the system land in the region of interest. To minimize simulation times and maximize the visual clarity of the results, this lower flux is selected, but the periods of high ember activity should and will be considered when discussing the results.

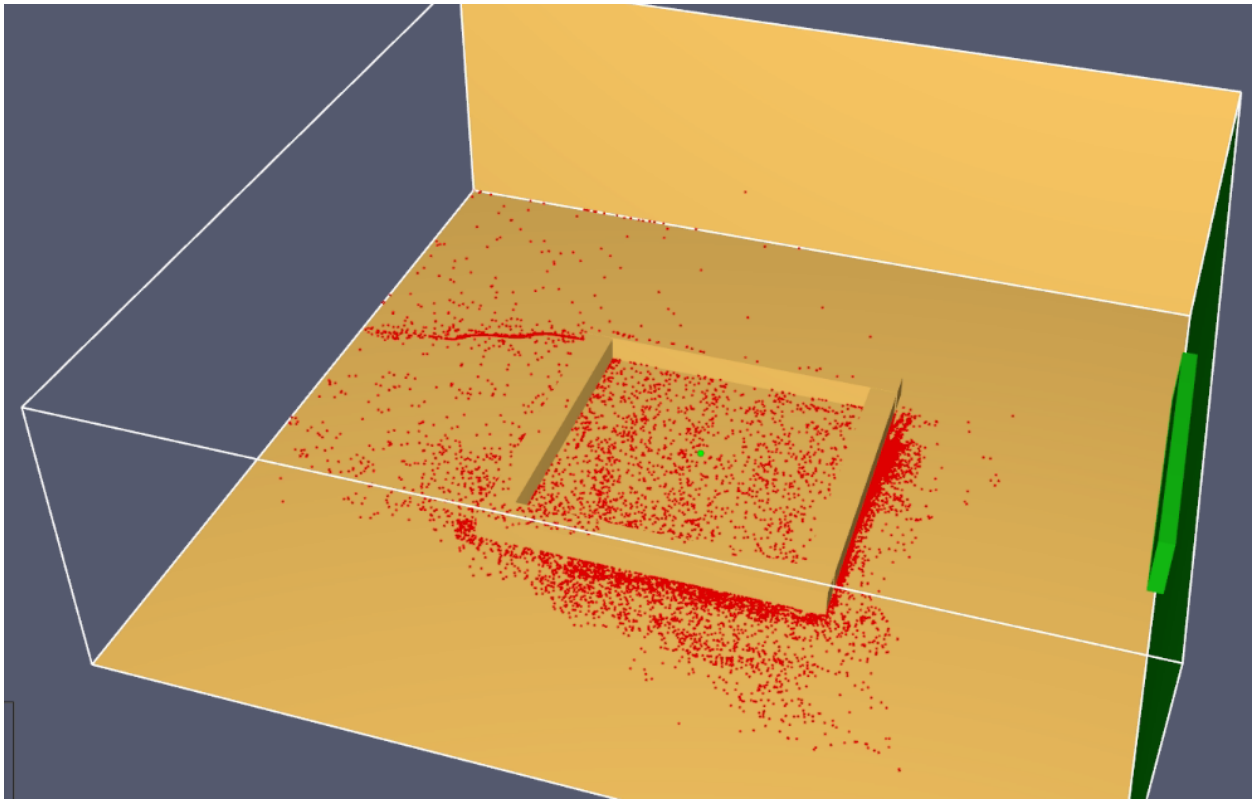

Figure 19: Procedure to Calculate Ember Flux

2.6. Meshing and Rasterization of Angled Objects

During preliminary trials, it was observed that angled objects (such as a roof) are rasterized to conform to FDS's grid-based geometry. Rasterization is limited by the fineness of the grid. This phenomenon was also captured in the earlier work during trials testing the effects of friction [6]. Therefore, one should note that ember accumulation in these experiments is dominated by

geometry above all else. Additionally, it was noted that embers accumulated in a large “step”pattern that is far from the surface of the structure and could cause some particles to vanish. See an example of a very coarse mesh in FIgure 20. Sufficiently small meshes eliminated this vanishing effect. Although PyroSim does not offer adaptive meshing, one can split meshes and refine the grid size in critical areas. Therefore, the grid around the homes is refined to 0.167 m and it is enlarged to 0.33 m as the distance once the distance from the home is sufficiently large. Ultimately, the house trial simulations contained approximately 450,000 nodes, which reduced or eliminated the shortcomings described above.

Figure 20: PyroSim’s Rasterization of Angled Objects

3. Results

3.1. Building Design

3.1.1. Roof Ember Accumulation

Each of the building designs is asymmetric and was tested multiple times with different orientations relative to the wind (recall, 5 m/s horizontal and 3 m/s vertical). For the two square cases, the 0° trial collected 2.52 grams (g) of embers on the roof and the 90° trial collected 3.01 g. In the 90° trial, where there was slightly greater accumulation, the ridge line (defined where each half of the sloping roof meets) was perpendicular to the wind direction.

For the two rectangular cases, the 0° trial collected 1.18 g of embers and the 90° trial collected 1.27 g. These trials had relatively little accumulation relative to the square case, but it is important to note that this model occupies only half the area as the square. Later, ember mass per unit area for each house will be calculated to compare concentrations. Again, the ridge line was perpendicular to the wind in the 90° trial, where there was greater accumulation.

For the two L-Shape cases, the 0° trial collected 1.99 g of embers and the 90° trial collected 2.58 g. In this design, regardless of orientation, there is an equal amount of ridge line parallel and perpendicular to wind speed. However, the 90°configuration has the perpendicular ridgeline at the leading edge of the house, closest to the ember cloud, and the 0° configuration has the ridgeline at the tail edge of the house.

For the three T-Shape cases, the 0° trial collected 1.83 g of embers, the 90° trial collected 1.98 g, and the 180° trial collected 3.02 g. Both the 0° and the 180° trials have a dominant ridgeline perpendicular to the wind. However, the 180° configuration has the ridgeline and broad side of the building at the leading edge of the house, closest to the ember cloud.

For the two IBHS Replica cases, the 0° trial collected 1.97 g of embers and the 90° trial collected 2.64 g. This roof design is more complex, but in the 90° trial, the primary ridge line of the roof is perpendicular to the wind, and again, collects more embers. Figure 21, below illustrates PyroSim's visual output of ember accumulation and mass concentrations. See section 6.6 of the appendix for images of each trial listed above.

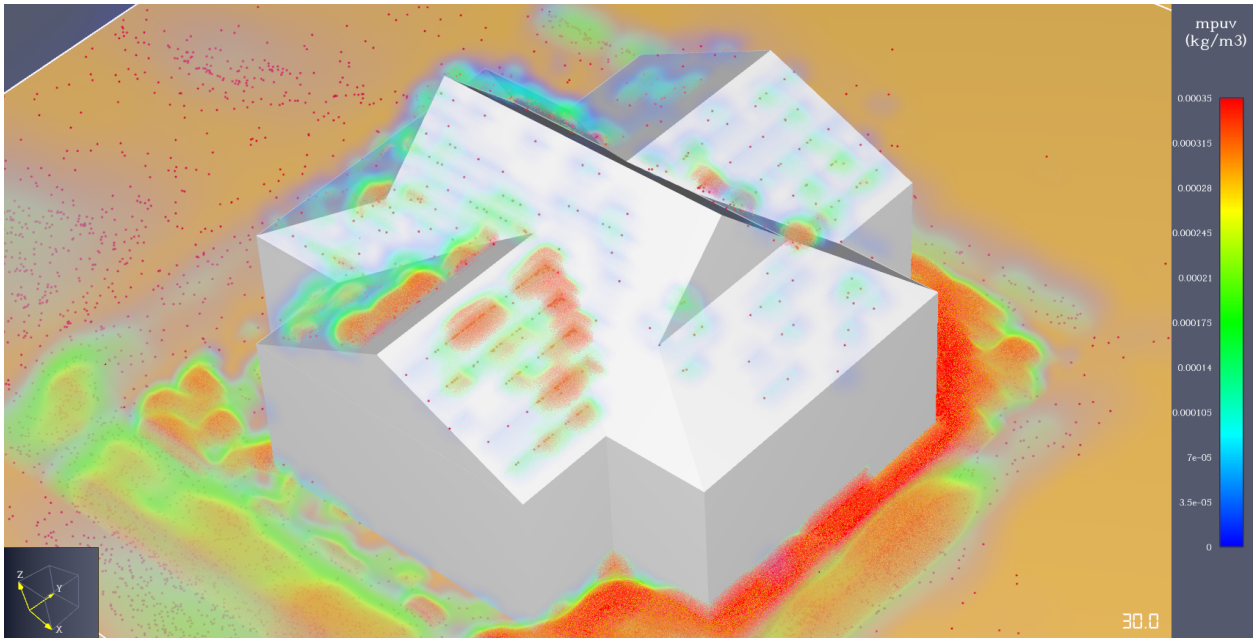

Figure 21: IBHS 90° Ember Accumulation

From the data above, it is clear that in order to minimize ember accumulation on a roof for a given building design, the structure should be built with a ridge line that is parallel to expected wind directions. See Table 5 and Figure 22 for a clear summarization of this fact. In PyroSim's geometry-based system, embers can slide off parallel ridge roofs more easily, as opposed to getting trapped in the steps that form the perpendicular roof. Additionally, one can calculate the average mass per unit area of all trials for a given building design. Doing so, the result is, interestingly, that the roof shape tends to have a somewhat limited effect on mass accumulation, but that orientation is consistently important. Examining the simulation results, embers tend to concentrate on internal roof corners, valleys, and other complex shapes. However, the ridgeline is the dominant determiner of mass accumulation on a roof.

Table 5: Building Design Mass Accumulation on Roof

Building Design	Mass [kg]	Mass per Area [kg/m^2]
Square (0°)	0.00251	2.51E-05
Square (90°)	0.00301	3.01E-05
Rectangular (0°)	0.00118	2.36E-05
Rectangular (90°)	0.00127	2.54E-05
L-Shaped (0°)	0.00199	2.65E-05
L-Shaped (90°)	0.00258	3.44E-05
T-Shaped (0°)	0.00183	2.44E-05
T-Shaped (90°)	0.00198	2.64E-05
T-Shaped (180°)	0.00302	4.03E-05
IBHS Replica (0°)	0.00197	2.35E-05
IBHS Replica (90°)	0.00264	3.14E-05

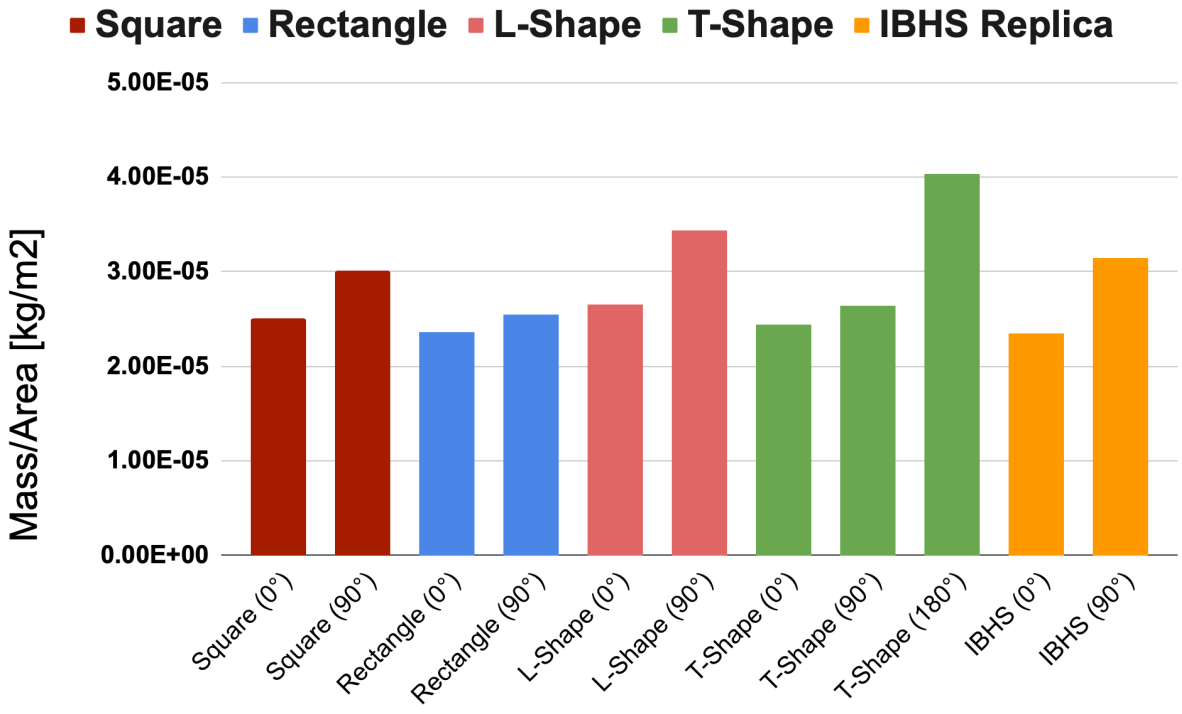

Figure 22: Effect of Building Shape on Mass Accumulation on Roof

3.1.2. Zone 0 Ember Accumulation

Recall that Zone 0 is the defensible space extending ~1.5 m from the walls of the residential building. Although it's not required by law, many fire experts call this ember-resistant zone the

most important in preventing fire from spreading to homes. Here, we examine the total mass that came to rest in Zone 0 for each trial on a kilogram basis and as a percent of total mass entering the system. As one might expect, the total mass accumulation for each trial, regardless of orientation, is similar. This is because the houses essentially behave like a 10 m wall that collects all embers on the front side with some contributing mass along the sides or back due to flow stagnation or recirculation. However, the major takeaway is that, for each trial, approximately 20% of all embers introduced into the system came to rest in Zone 0, emphasizing why this region should be kept clear of any ignition sources.

Table 6: Ember Accumulation in Zone 0

Building Design	Mass [kg]	Percent of Total
Square (0°)	.0220	20.26%
Square (90°)	.0182	16.76%
Rectangular (0°)	.0261	24.03%
Rectangular (90°)	.0218	20.07%
L-Shaped (0°)	.0207	19.06%
L-Shaped (90°)	.0231	21.27%
T-Shaped (0°)	.0223	20.53%
T-Shaped (90°)	.0228	20.99%
T-Shaped (180°)	.0254	23.39%
IBHS Replica (0°)	.0209	19.24%
IBHS Replica (90°)	.0206	18.97%
Average	**.0221**	**20.45%**

3.2. Varying Horizontal Wind Speed

To test the effects of wind speed, the IBHS Replica house (90°) was subject to eight trials of varied horizontal wind speed (the vertical speed of 3 m/s remained constant to introduce artificial turbulence and facilitate transport). This house design and orientation was selected because the design is the most complex and has a history of use in fire research. Here, mass accumulation on the roof is measured. The 90° orientation was selected because this configuration was more likely to capture embers and thus provide a meaningful range of results. At 2.5 m/s, the wind was not sufficient to carry the particles, and the embers deposited on the ground before ever reaching the house. For the 3.75 m/s, 5 m/s, and 6.25 m/s cases, the ember mass on the roof was 0.624 g, 2.64 g, and 2.73 g, respectively. Ember accumulation increased with each trial. For the 7.5 m/s, 10 m/s, and 12.5 m/s cases, the ember mass on the roof was 1.65 g, 0.844 g, and 0.785 g, respectively. Therefore, ember accumulation decreased with each trial.

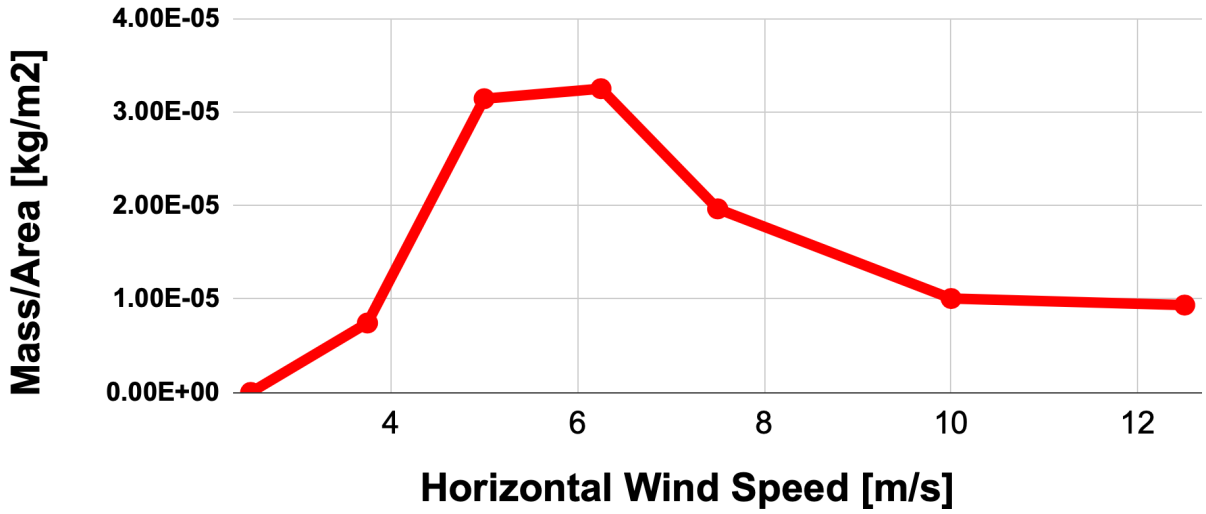

Figure 23: Horizontal Wind Speed Trials over IBHS 90°

The results indicate that there is a minimum wind speed necessary to facilitate the transport of embers and a maximum speed at which embers can meaningfully deposit and remain on the roof. According to this data set, the critical wind speed for ember accumulation on the roof would be approximately 6 m/s. From visual observations of wind speed trials, it is clear that the structures create streamlines and form a flow separation layer that embers have a difficult time crossing. This layer becomes stronger at higher wind speeds and very few embers even break through and have the chance to deposit on the roof. Additionally, those that do deposit are more likely to continue moving along the roof's surface until they are blown off the side or back rather than remaining at rest.

3.3. Fire Effects on Benchmark Turbulent Flow

Here, we return to the mock wind tunnel simulations used to validate PyroSim's LES calculations in Section 2.1. We verified that the turbulent flow before and around the cube behaved as expected. Now, we leverage PyroSim to create a fire upstream of the cube and examine the velocity fields and vorticity contours to determine the effects the fire has on the results.

To begin, we define a reaction in PyroSim and use the preset chemical composition and byproducts for pinewood because it is a common fuel for forest fires. This reaction can simply be applied to any surface and that surface will output the heat and byproducts defined by the reaction. Additionally, the heat release rate is selected to be 1000 W/m^2, which is a very high flux, but this is done to magnify any changes in flow that heat from a fire may create. Recall that the cube in Section 2.1 had a side length of h, otherwise 0.1 m. Now, we model a smaller cube of side length 0.02 m and place it a distance, h, upstream of the original cube. We apply the reaction surface conditions to the cube and ensure the cube lacks any physical properties, meaning that fluid can pass through it without inherently disrupting the flow. The velocity

vector fields in the x-z and y-z plane will be included in section 6.7 of the Appendix, but changes in the flow field are particularly difficult to decipher from those plots. Contours of the x and y components of mean vorticity are pictured below.

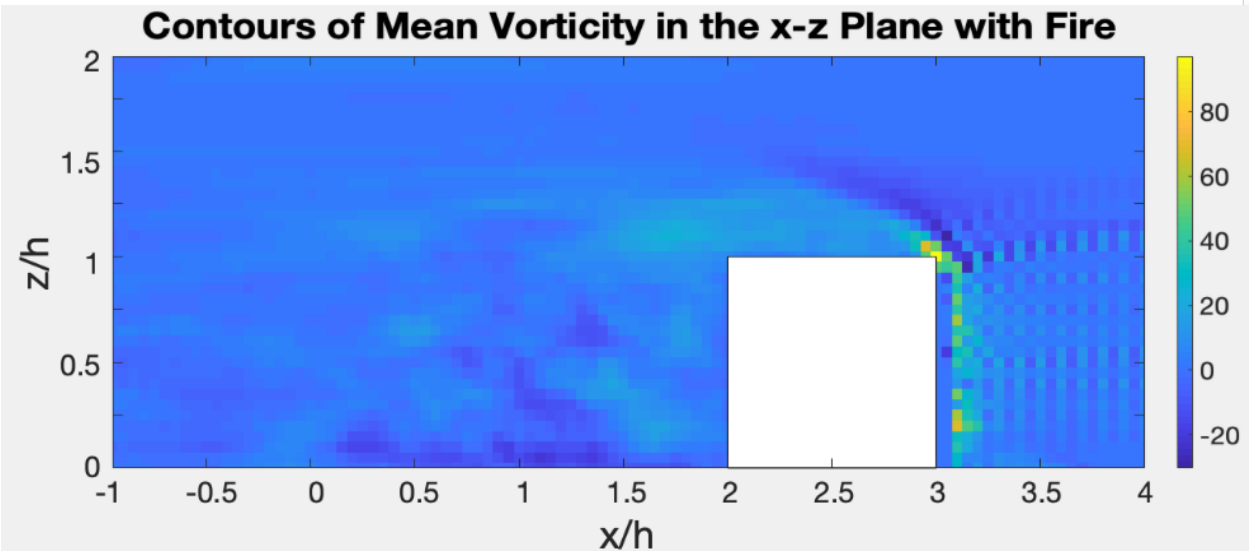

Figure 24: Contours of Mean Vorticity (ω_y) with Upstream Fire

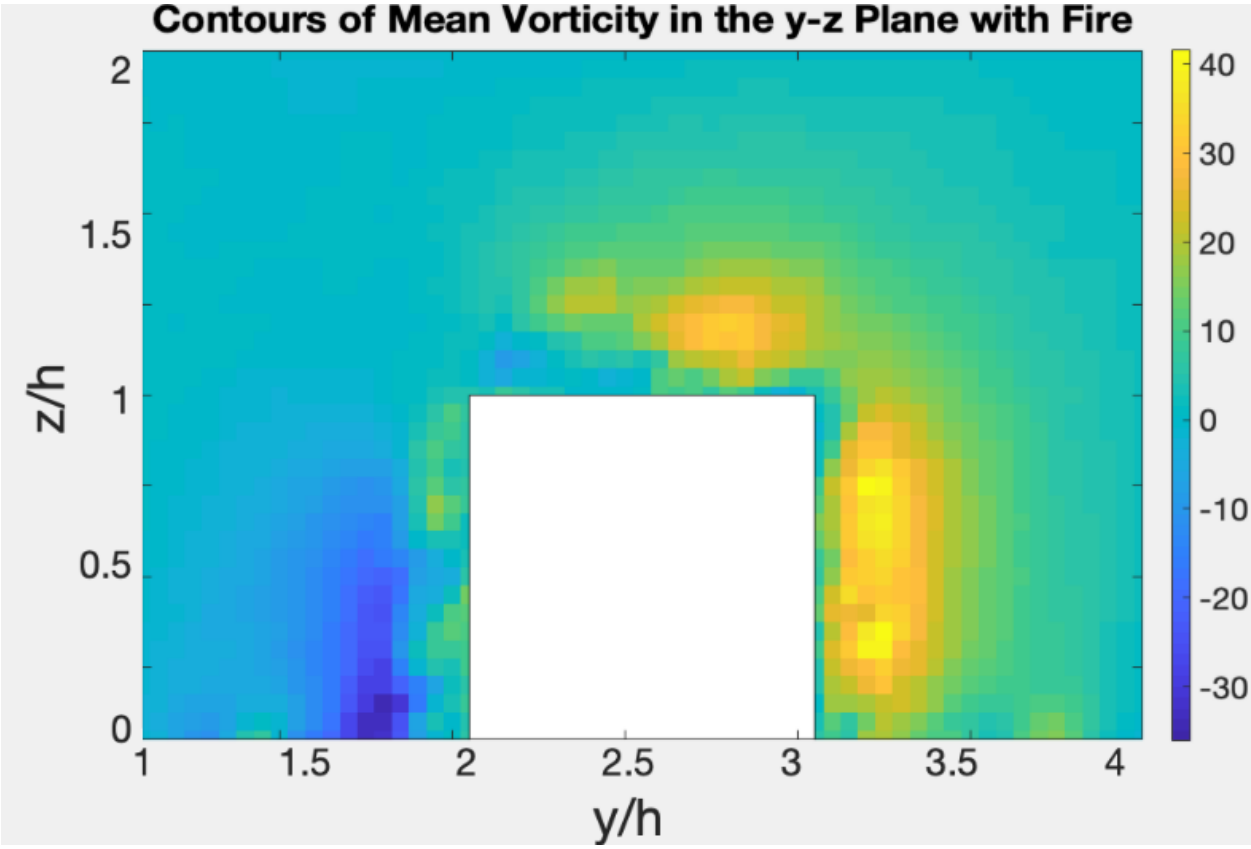

Figure 25: Contours of Mean Vorticity (ω_x) with Upstream Fire

At first glance, the vorticity contours appear identical to the non-fire case. While they are very similar, some changes become apparent if we take the difference in vorticity between the fire and non-fire cases. See Figures 26 and 27, below, to confirm that the vorticity around and in the wake of the cube undergoes fluctuations due to the introduction of the fire.

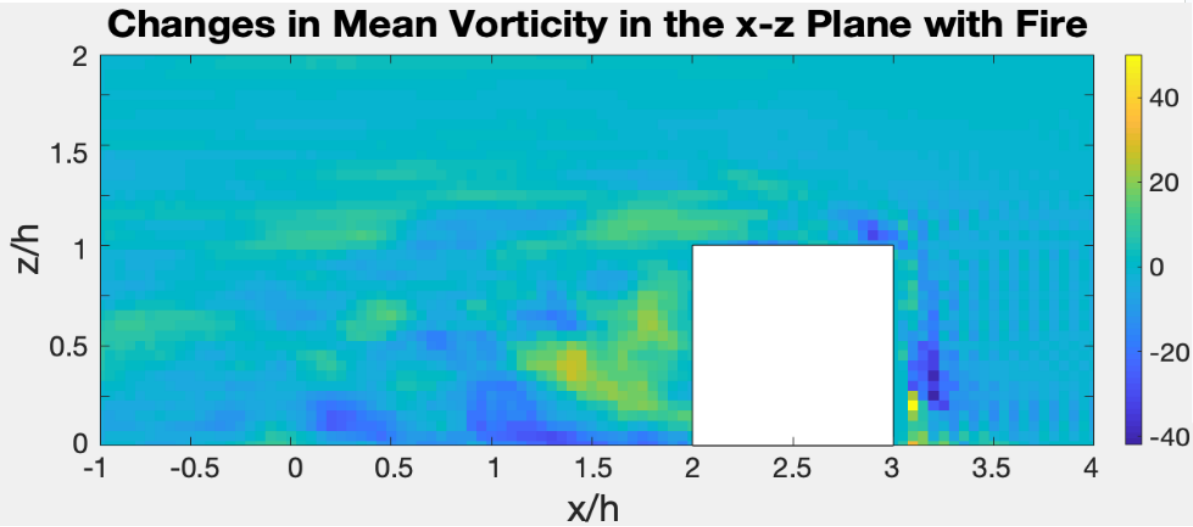

Figure 26: Changes in Mean Vorticity (ω_y) Contour with Fire

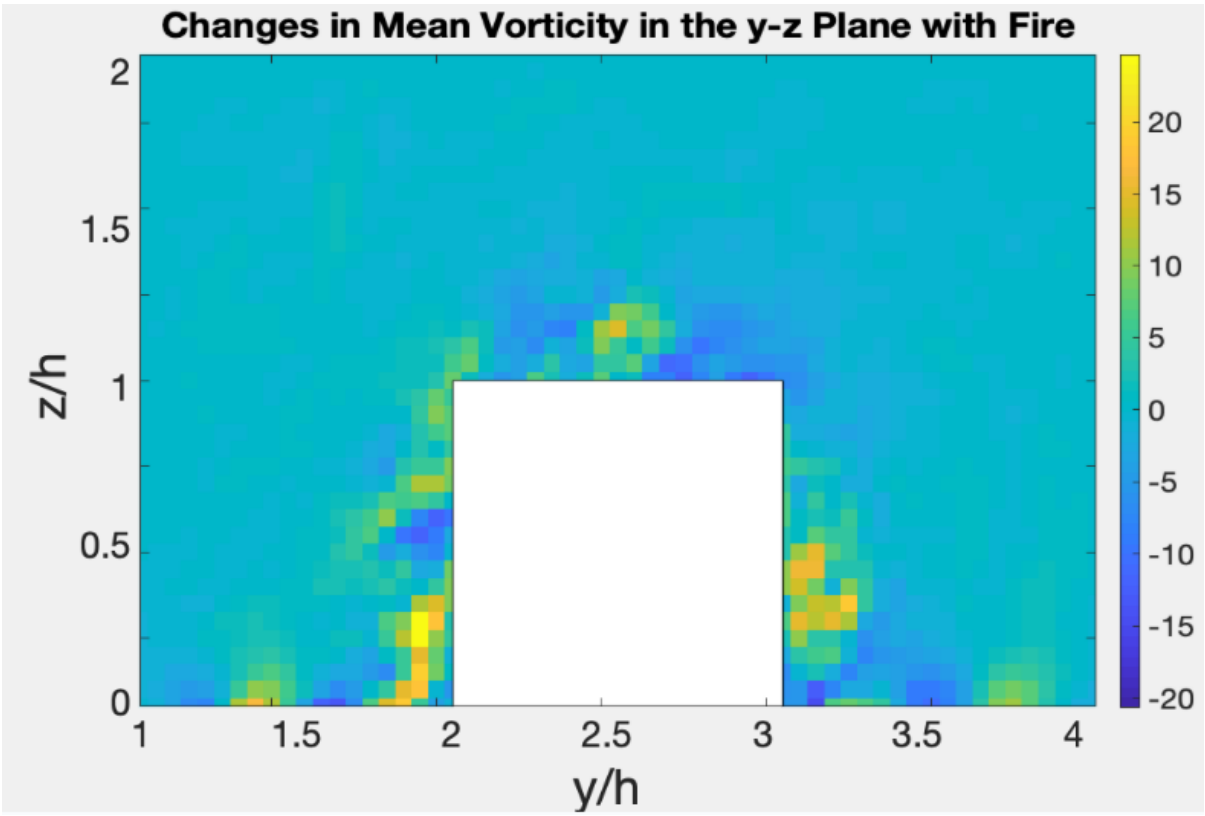

Figure 27: Changes in Mean Vorticity (ω_x) Contour with Fire

The procedure described above was repeated for two additional trials. In Case 2, the heat release rate of the fire was increased to 3000 W/m^2 to determine if a greater intensity magnified the changes in vorticity. However, this did not have an effect notably greater than the initial case with a lower heat flux. In Case 3, the heat flux was dropped back down to 1000 W/m^2 but the fire was moved to a distance h/2 from the leading edge of the cube. This trial did not have a noticeable effect on the change in vorticity relative to the first case either. For reference, changes in vorticity for these additional trials are included in the Appendix.

3.4. Fire Effects on Ember Accumulation for Model Home

Ultimately, the findings in Section 3.3, above, indicate that introducing fire to the larger simulation with the model homes may impact results because vorticity dynamics, and thus turbulence were affected. Changes in turbulence could potentially impact how embers travel, behave in the air, and settle. As such, we return to the simulation with the IBHS 90° home but introduce a ground fire along the length of the inlet, below the ember infection site. Defensible Zone 2 limits major combustible debris, but a ground fire is a possibility. Here, we again select the default pine reaction in PyroSim. However, the heat release rate input is lowered to 40 W/m^2, which is a flux that has been observed by burning pine debris in literature [19]. The updated model is depicted in Figure 28. The red strip at the inlet denotes the ground fire. The fire is given 5 seconds to ramp to maximum intensity before embers are released into the system.

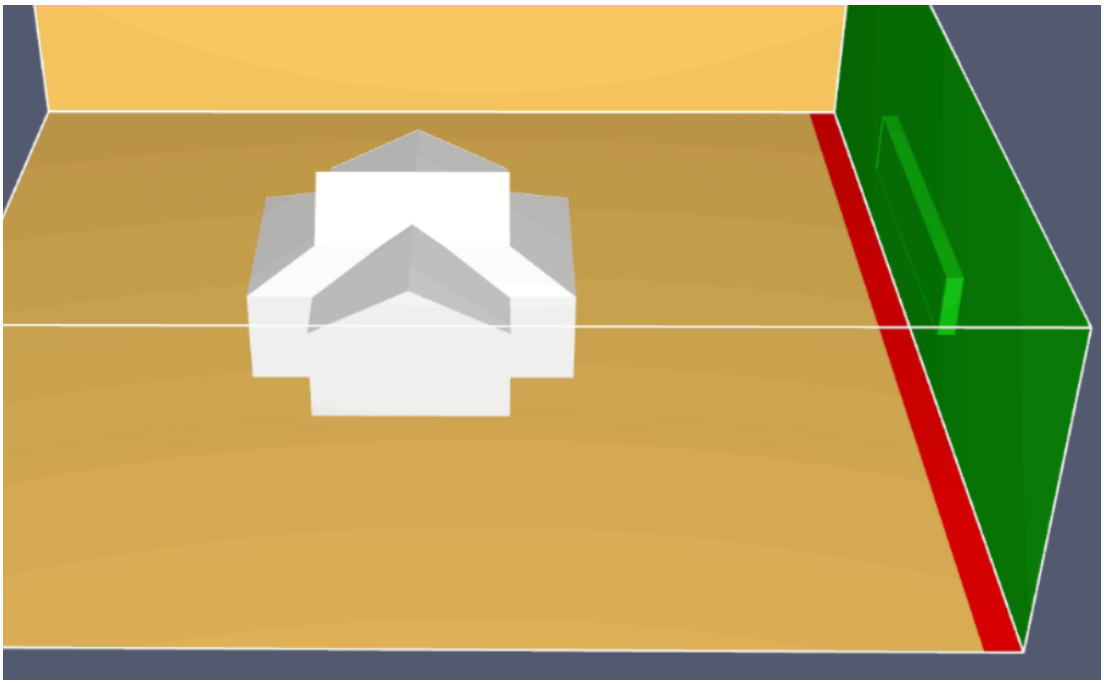

Figure 28: Model Setup with Ground Fire

First, the existing trial for the IBHS 90° home was repeated with no parameters changed aside from the fire. The horizontal wind speed was 5 m/s and the vertical wind speed was 3 m/s. Interestingly, the ember accumulation on the roof dropped to 2.28 g from 2.64 g. This may suggest that the fire's impact on vorticity and turbulence made it more difficult for embers to come to rest on the rooftop.

Following that test, the vertical wind speed was dropped to 0 m/s to determine if the plume produced by the ground fire was capable of lifting embers for long-distance transport without the artificial vertical velocity component. Horizontal wind speed was held constant at 5 m/s. In the trial with no fire and no vertical wind, the mass accumulation on the roof was 1.47 g. Contrary to the previous example, introducing fire increased mass accumulation on the roof to 2.27 g.

Finally, trials were conducted with a horizontal wind speed of 5 m/s and a vertical wind speed of 5 m/s to determine if the fire's turbulence impacted instances with strong lofting winds. This approach also introduces a third data point to further define a trend in the results. In the trial with no fire, the mass accumulation on the roof was 6.15 g. Here, the presence of fire decreases ember mass on the roof to 4.64 g.

Table 7: Effects of Ground Fire on Mass Accumulation on Roof

Ground Fire	Vertical Wind Speed	Roof Mass [kg]	Fire Effect
No	0	0.00147	Increases accumulation by 54.4%
Yes	0	0.00227	
No	3	0.00264	Decreases accumulation by 13.6%
Yes	3	0.00228	
No	5	0.00614	Decreases accumulation by 24.4%
Yes	5	0.00464	

Although these findings appear incongruent, there is a possible explanation. In the absence of the artificial vertical wind used to loft the particles and generate turbulence, the fire-driven wind carries the particles and allows them to travel to the roof. On the other hand, when the vertical component of wind speed is present, the fire may or may not be needed to loft the particles. The assumption is that the fire creates more turbulent air and introduces vortices and recirculation patterns that may mitigate the number of embers settling on the roof.

3.5. Spatial Temperature Data

Finally, we take spatial temperature data along key sections of the model at the end of the ember injection phase. One goal here is to compare an instance with fire and no fire to see if

the embers or the fire at the injection site is the dominant mode of heat transfer to the homes. One trial will be done without a fire, and another will be performed with the ground fire. The other goal is to examine points of maximum temperature and determine if they pose a risk to building materials or other ignition sources on or around a house. Thus far, ember parameters for properties related to heat transfer have not been discussed. However, the ember parameters were selected as follows. The initial temperature is set at 850°C, which is the average temperature of firebrands referenced in a paper measuring heat transfer between firebrands and other surfaces [20]. Additionally, the thermal conductivity and specific heat were input as 0.1 W/mK and 2 kJ/kgK, respectively, according to a paper studying the thermal contact of glowing firebrands [21].

In the trial with no ground fire, temperature profiles failed to exceed 20°C which is the ambient air of the model. This remained true throughout the model, even against the front wall of the house, where embers collected in mass. This indicates that PyroSim does not calculate the spatial heat emitted by the ember particles to the environment. Future work could be performed in PyroSim to simulate how the piles of embers might transfer heat to the environment or nearby surfaces. In the trial with the ground fire, temperature increases were minimal but present. The maximum temperature along the house was approximately 25°C. This is because the roughly 10-meter Defensible Zone 1 worked as intended and limited fire spread via direct flame contact or radiant heat. Temperature profiles over key sections of the model for the case with the ground fire are displayed in Figures 29 and 30, below. Heat accumulates along the front edge of the home that is most exposed to the flame.

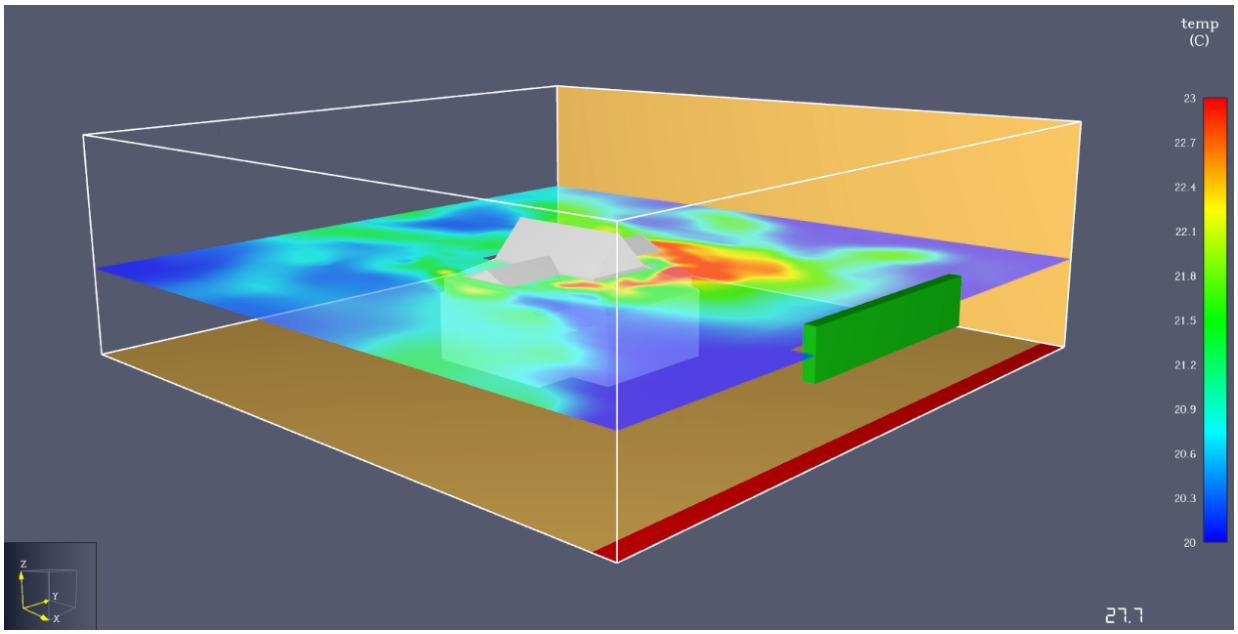

Figure 29: X and Y axis Temperature Profiles due to Ground Fire

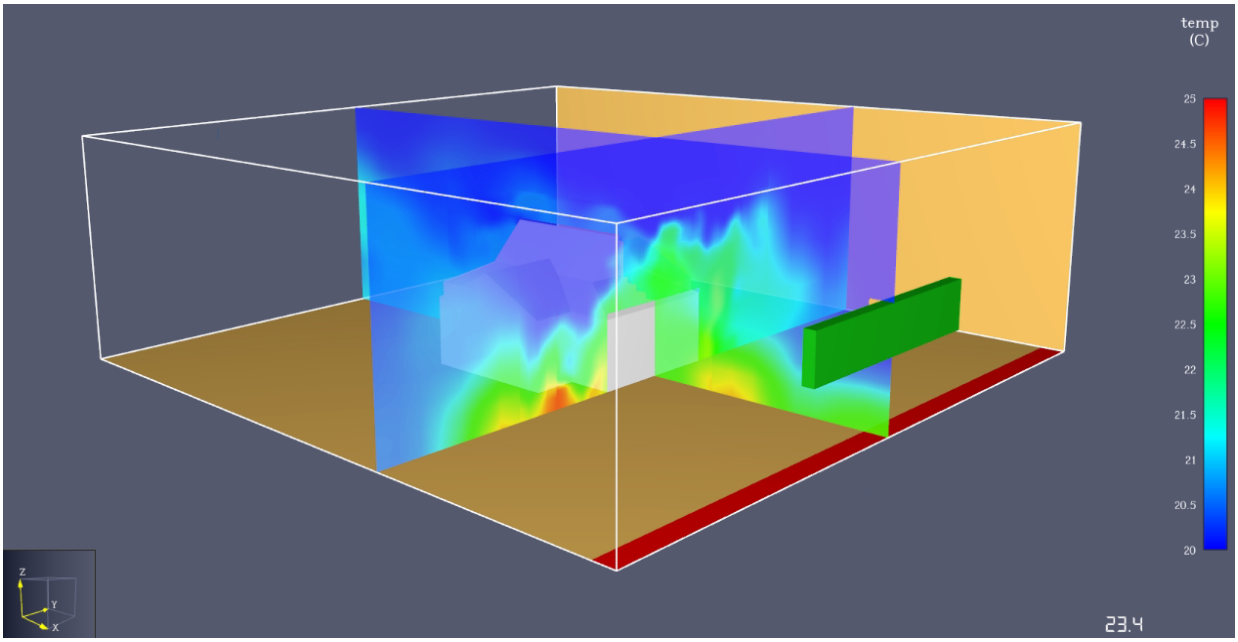

Figure 30: Z-axis Temperature Profile due to Ground Fire

4. Discussion and Conclusions

4.1. Discussion: Highlights, Shortcomings, Future Work

One important point to reiterate is that PyroSim's grid-based geometry leads to the results being dominated by the rasterized steps formed by the angled roof. Although friction is present, its effects are pushed to the side. Additionally, in a real-world scenario, hot embers can melt roof material and create additional surface forces preventing movement. This study examined only isolated buildings with simple wall and roof designs. Further trials could examine how building features such as vents, balconies, decks, or gutters create additional accumulation patterns. Buildings in the real world are often not isolated, and the turbulence and streamlines generated by nearby structures, whether manmade or vegetative, could drastically impact how embers behave and deposit onto nearby buildings.

Several points of discussion revolve around the embers themselves. For example, the embers were limited to one shape, size, and density. A highly advanced CFD software may allow one to create multiple ember clouds that generate spheres, discs, and cylinders of different sizes to more realistically model the distribution and transport of embers during a real fire. Unfortunately, PyroSim cannot handle the complex drag forces or moments of inertia associated with non-spherical shapes. In the real world, small spherical embers such as these are unlikely to be the primary source of fire spread. Typically large flat discs of much greater mass can take flight and propagate wildfire spread. Recall Section 2.5.3 on ember count. To reduce clutter and minimize simulation time, an ember flux of just 1.15 pcs $m^{-2}s^{-1}$ was selected. While this falls within a range cited in the literature, it is important to note that a follow-up study found the flux to be as high as 7 pcs $m^{-2}s^{-1}$ when periods of very low ember activity are removed. As such, each of the mass values described in this report could theoretically be seven times greater. Ultimately, the report is not trying to perfectly replicate ember mass accumulation observed in the field. While parameters are selected to maximize realism, the embers need to be small to facilitate transport, so the primary goal is to identify trends and accumulation patterns that would likely translate to larger, more dangerous embers.

A very interesting section of the report with lots of room for growth is the examination of fire effects on the benchmark flow field. Not only did it confirm that fire alters the velocity, vorticity, and turbulence of a flowing system, but also that PyroSim can capture those changes. Oddly, the variations in fire intensity and position in Section 3.3 did not appear to significantly affect flow compared to the baseline case. This may be attributed to the fire requiring more time to fully develop and impart its effects onto the surrounding flow. The vector and vorticity fields were calculated using mean data. The effects of fire may have been even more profound if fluctuations were observed on a temporal basis.

4.2. Conclusions

Based on all of the trials described above, there are several major conclusions. First, regardless of building shape, ember accumulation is greater when the predominant ridge line of the roof is

perpendicular to the wind direction. Second, embers that deposit on a roof tend to accumulate in internal corners, valleys, or against sloped surfaces. These complex structures may create turbulence that allows embers to more easily reach the surface and then come to a stop when they hit a geometric dead end. Despite this, the roof shape led to outcomes that were tough to rationalize, with all trials producing mass accumulation rates of similar magnitude. Alternatively, the orientation of the roof turned out to be more consistent and predictable in determining accumulation rates. Third, for embers to accumulate, the wind speed must strike a balance between facilitating ember transport and allowing embers to deposit on the surface. This critical wind speed may maximize ember deposition in dangerous regions. Fourth, embers get trapped and accumulate in great quantities around the base of the building, particularly on sides facing the wind. Although " Defensible Zone 0" (0 to 5 ft from the structure) is not mandated by law, keeping this area clear of fuel is of incredible importance in preventing fire spotting near buildings. Typically, 20% of embers injected into the system piled up in Zone 0. The mass of embers here is statistically significant enough to transfer fire to any uncleared combustibles such as debris or outdoor furniture.

Another important finding in PyroSim is that introducing a fire to a system alters the velocity field and vorticity contours, even if all other parameters are left unchanged. These changes are particularly noticeable directly around an obstructive body and in its wake. When a ground fire was applied to the simulation of an ember storm passing over a model home, it had very unique impacts on the results. We posit that a fire can induce winds that help elevate particles in an otherwise streamlined flow field. However, this same force that lofts particles may also be liable to prevent them from coming to rest. Overall, the turbulent effect of fire on wind is a very complex subject with many competing factors that are difficult to predict. Finally, PyroSim fails to capture how the hot particles transfer heat to the surrounding air. The embers had no impact on environmental temperature measurements. However, PyroSim successfully captured the effects of manually designed fires applied to surfaces of the model, as observed by temperatures above ambient in trials with a ground flame at the inlet.

5. References

1. Leverhulme Wildfires Centre. The Fastest and Most Complex Wildfire Spread Pathway: Firebrand Spotting. 2022. https://centreforwildfires.org/news/the-fastest-and-most-complex-wildfire-spread-pathway-firebrand-spotting/

2. Defensible Space - Ready for Wildfire. Cal Fire. **2019.** https://www.readyforwildfire.org/prepare-for-wildfire/get-ready/defensible-space/

3. Defensible Space Zones. Fire Safe Margin. **2023.** https://firesafemarin.org/create-a-fire-smart-yard/defensible-space/defensible-space-zones/#gsc.tab=0

4. Standohar-Alfano Christine D., Estes Heather, Johnston Tim, Morrison Murray J., et al. Reducing Losses from Wind-Related Natural Perils: Research at the IBHS Research Center. *Frontiers in Built Environment.* **2017**. Volume 3. www.frontiersin.org/articles/10.3389/fbuil.2017.00009

5. Dac Nguyen, Nigel B. Kaye, Quantification of ember accumulation on the rooftops of isolated buildings in an ember storm, *Fire Safety Journal*, Volume 128, 2022, 103525, ISSN 0379-7112, https://doi.org/10.1016/j.firesaf.2022.103525

6. Rishub Shah. Ember Accumulation during Wildfires. *Young Scientists Journal.* 2020. https://ysjournal.com/engineering/ember-accumulation-during-wildfires/

7. PyroSim Users Manual. *Thunderhead Engineering.* https://support.thunderheadeng.com/docs/pyrosim/2020-5/user-manual/

8. Monika Nitsche. Vortex Dynamics. *University of New Mexico.* Vortex DynamicsUniversity of New Mexicohttps://www.math.unm.edu › ~nitsche › pubs

9. Hee Chang Lim, T.G. Thomas, Ian P. Castro. Flow around a cube in a turbulent boundary layer: LES and experiment. *Journal of Wind Engineering and Industrial Aerodynamics*. Volume 97, Issue 2. **2009**. Pages 96-109. https://www.sciencedirect.com/science/article/pii/S0167610509000117

10. Boundary Layer Thickness. *Wikipedia.* https://en.wikipedia.org/wiki/Boundary_layer_thickness

11. Vorticity | Applied Mathematics. *University of Waterloo.* https://uwaterloo.ca/applied-mathematics/current-undergraduates/continuum-and-fluid-mechanics-students/amath-463-students/vorticity

12. Emily Medlock. Standard Ceiling Height in the 21st Century. *HomeEdit - Architecture.* **2022**. https://www.homedit.com/standard-ceiling-height/

13. Common Roof Pitch. *B & M Roofing*. https://bmroofing.com/common-roof-pitch/

14. P. Cantor, M.R.T. Arruda, J. Firmo, F. Branco. Development of a standard firebrand accumulation temperature curve for residential wildfire protection system. *Results in Engineering*. Volume 17. **2023**. 100935, ISSN 2590-1230, https://doi.org/10.1016/j.rineng.2023.100935.

15. Samuel L M, Sayaka S. Influence of Angle Orientation on Firebrand Production from the Combustion of Surrogate Photovoltaic (PV) Panel Assemblies Exposed to Applied Wind Fields. *Fuel (Lond)*. **2020**. 279:10.1016/j.fuel.2020.118507

16. Alex W. Dye, John B. Kim, Karin L. Riley. Spatial heterogeneity of winds during Santa Ana and non-Santa Ana wildfires in Southern California with implications for fire risk modeling. *Heliyon*. Volume 6, Issue 6. **2020**. https://doi.org/10.1016/j.heliyon.2020.e04159.

17. Jan C. Thomas, Eric V. Mueller, Simon Santamaria, et al. Investigation of firebrand generation from an experimental fire: Development of a reliable data collection methodology. *Fire Safety Journal*. Volume 91. **2017**. 864-871,ISSN 0379-7112. https://doi.org/10.1016/j.firesaf.2017.04.002.

18. Bouvet, N., Link, E.D. & Fink, S.A. A new approach to characterize firebrand showers using advanced 3D imaging techniques. *Exp Fluids* 62, 181 (2021). https://doi.org/10.1007/s00348-021-03277-6

19. Martinka J, Rantuch P, Martinka F, Wachter I, Štefko T. Improvement of Heat Release Rate Measurement from Woods Based on Their Combustion Products Temperature Rise. *Processes*. 2023; Volume 11, Issue 4. https://doi.org/10.3390/pr11041206

20. Elias D. Bearinger, Jonathan L. Hodges, Fengchang Yang, Christian M. Rippe, Brian Y. Lattimer. Localized heat transfer from firebrands to surfaces, *Fire Safety Journal*, Volume 120. **2021**. 103037, ISSN 0379-7112, https://www.sciencedirect.com/science/article/pii/S0379711220300886

21. Alok Warey. Influence of thermal contact on heat transfer from glowing firebrands, *Case Studies in Thermal Engineering*. Volume 12. **2018**. Pages 301-311, ISSN 2214-157X, https://doi.org/10.1016/j.csite.2018.04.018.

6. Appendix

6.1. Reference Paper Turbulent Flow Around a Cube

First, we include the plots for the (u,w) vector field and the mean contour of the y-component of vorticity. The flow behavior from this report aligns well with the findings of the reference paper.

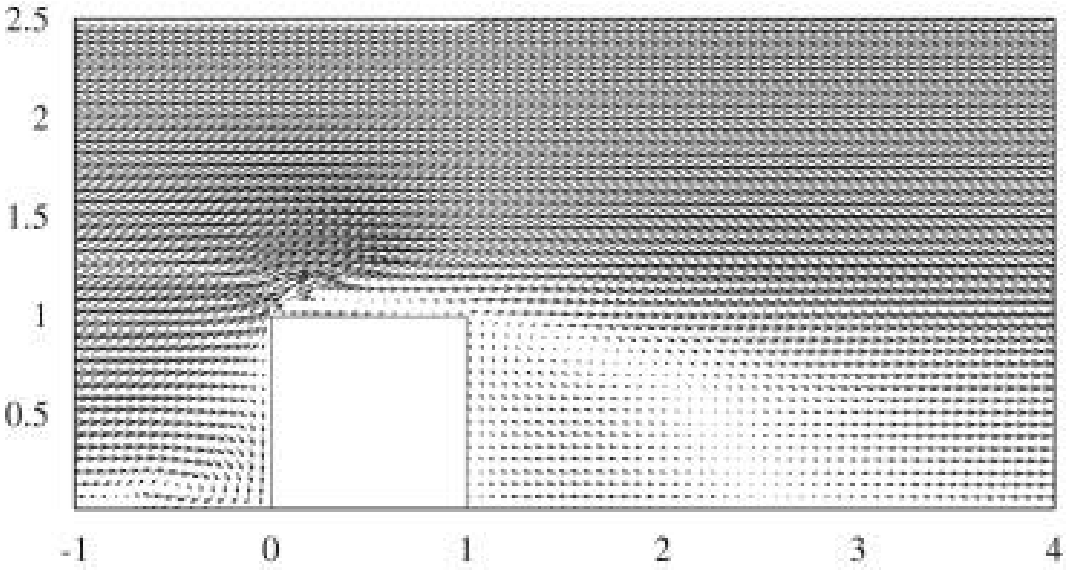

Figure A.1: Reference Velocity Vector field in x-z Plane [9]

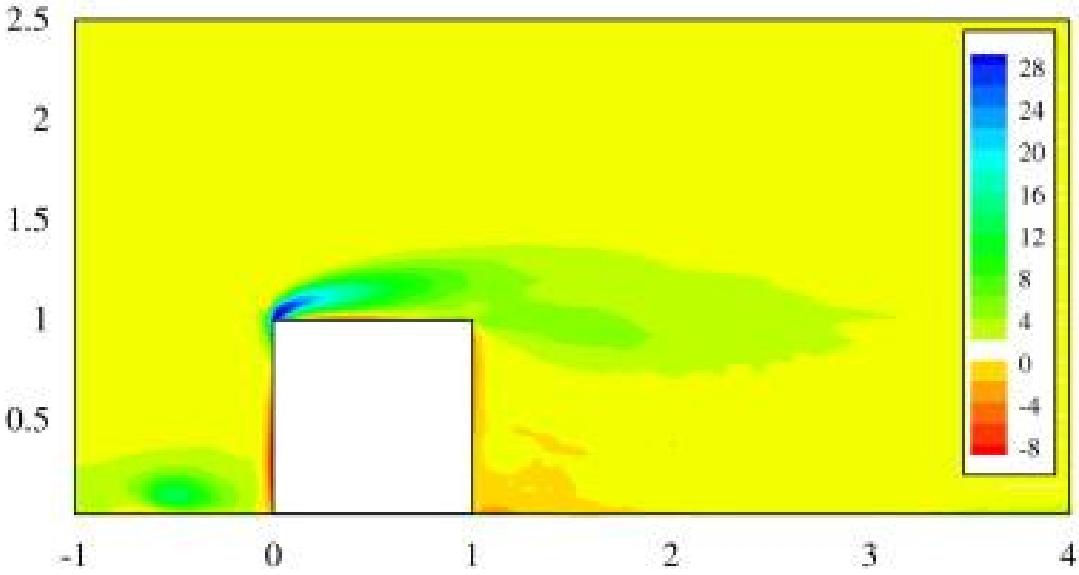

Figure A.2: Reference Vorticity Contour (ω_y) in x-z Plane [9]

Next, we include the reference plots for the (v,w) vector field and the mean contour for the x-component of vorticity. The flow behavior here aligns well with the findings in this report.

However, the reference vorticity plot may be onerous when compared with the vector field for the same data.

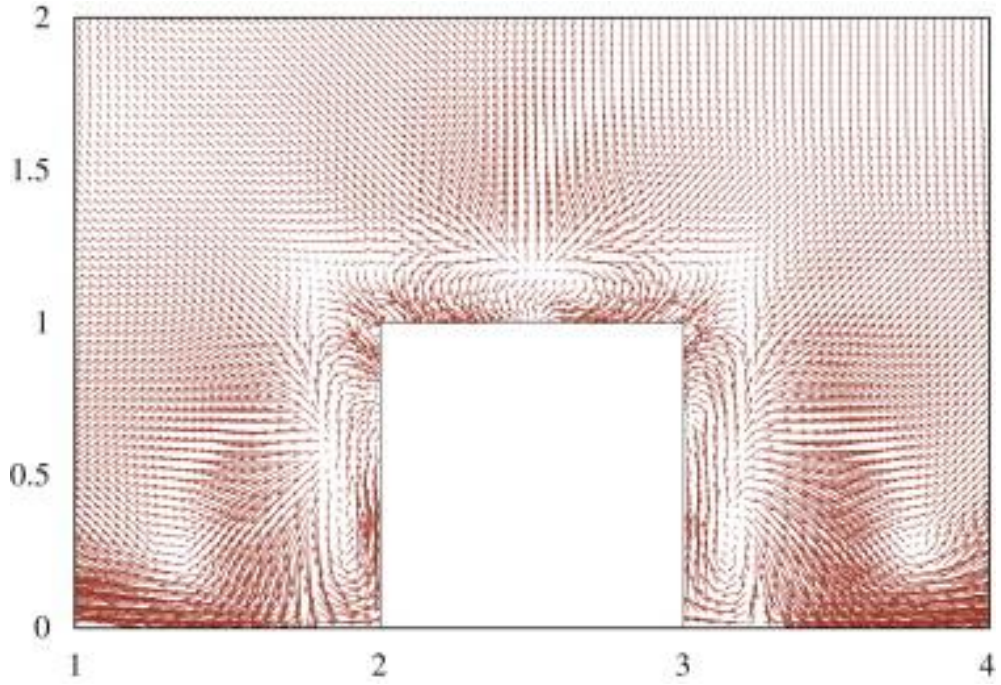

Figure A.3: Reference Velocity Vector Field in y-z Plane [9]

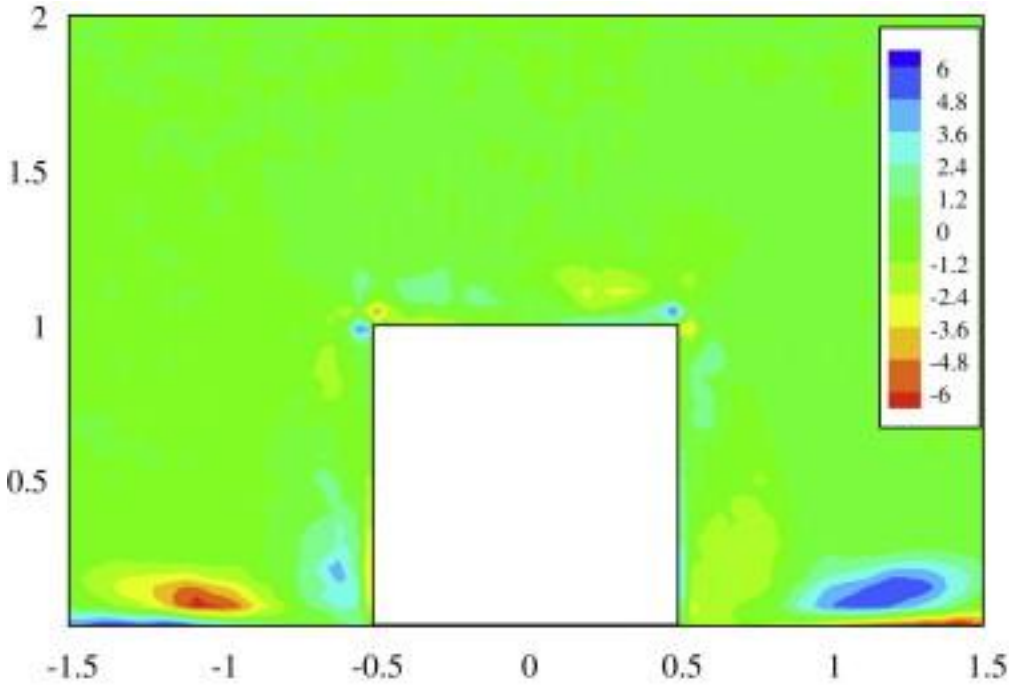

Figure A.4: Reference Vorticity Contour (ω_y) in x-z Plane [9]

6.2. Reference Paper Details of Cube Flow

Finally, we include the reference paper's results for streamwise and vertical velocity profiles along the axial centerline of the cube. The results are fairly similar, but one notable difference is the lower vertical velocity at the surface of the leading edge of the cube. This change can likely be attributed to slightly different boundary conditions of the cube used in this report. Ultimately, the results are similar and point to the validity of PyroSim in the simulation of turbulent flow over a bluff body.

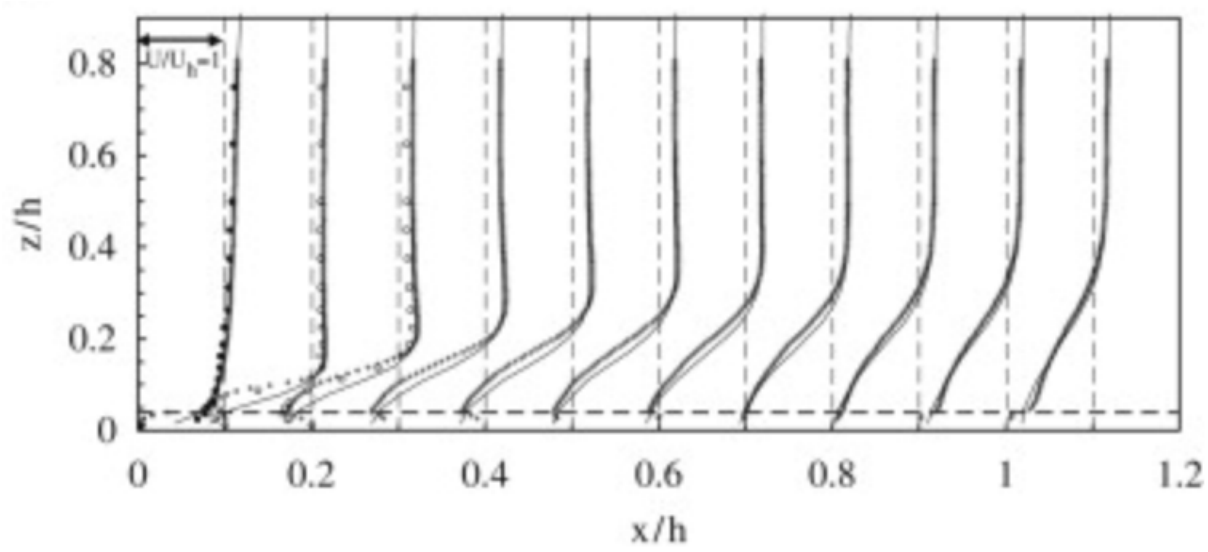

Figure A.5: Reference Streamwise Velocity Profiles over Cube [9]

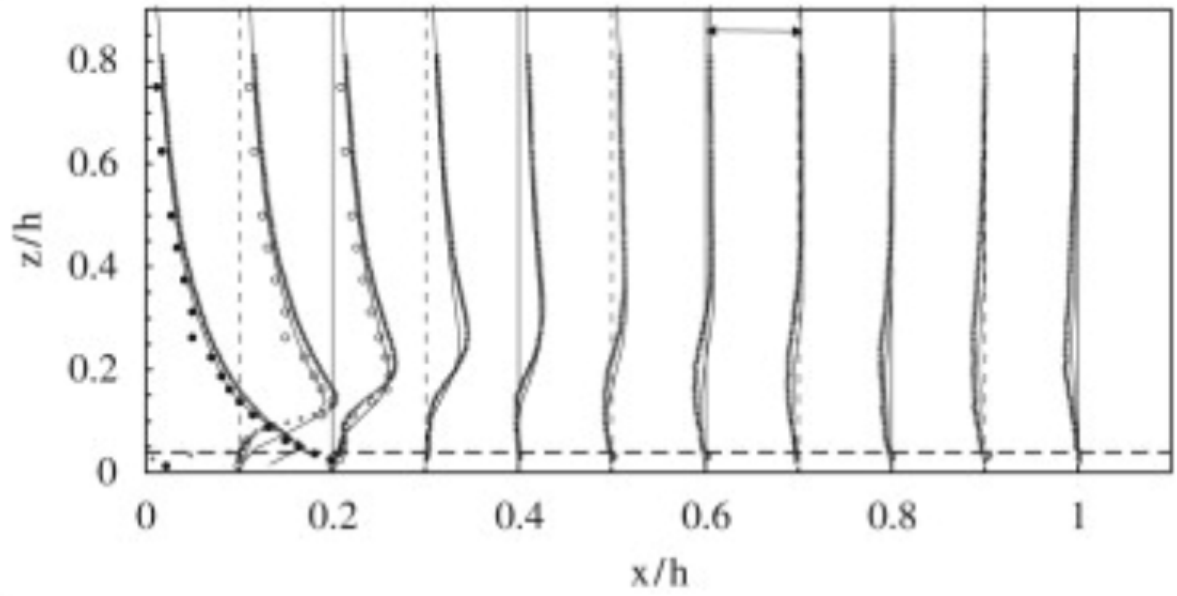

Figure A.6: Reference Vertical Velocity Profiles over Cube [9]

6.3. Model Home Dimensions

Building geometry and specific dimensions for the five model homes are pictured below.

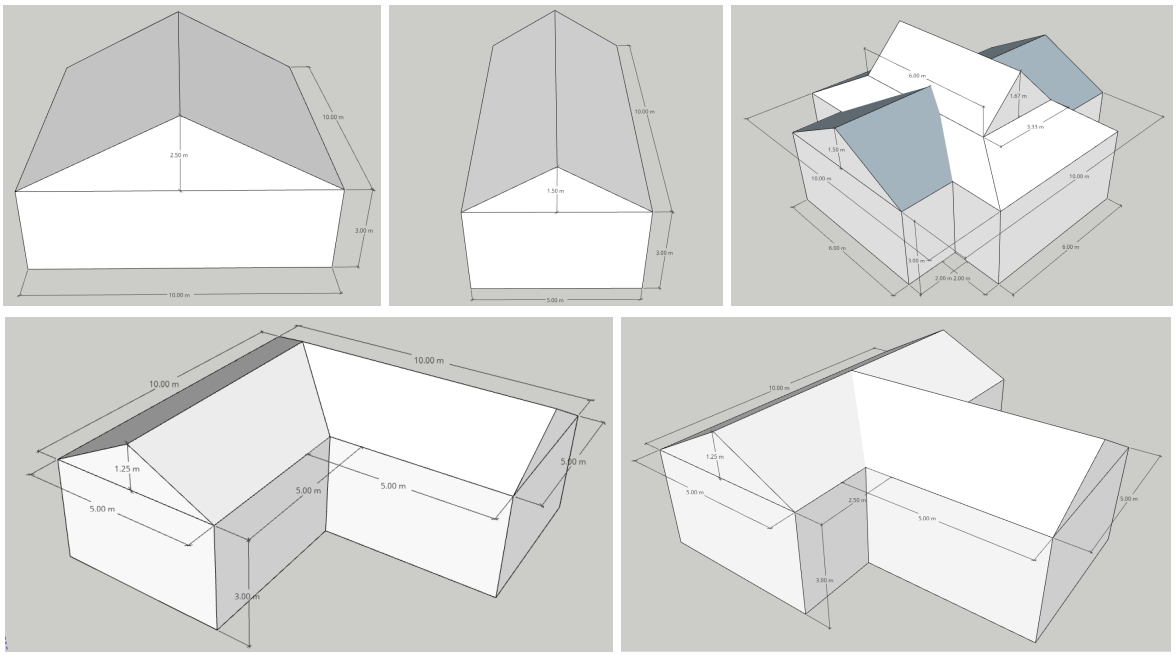

Figure A.7: Model Home Dimensions (Square, Rectangular, IBHS Replica, L-Shape, T-SHape)

6.4. Effects of Ember Size and Density - Additional Trials

The effects of ember radius on ember transport for the additional course mesh trials are pictured below.

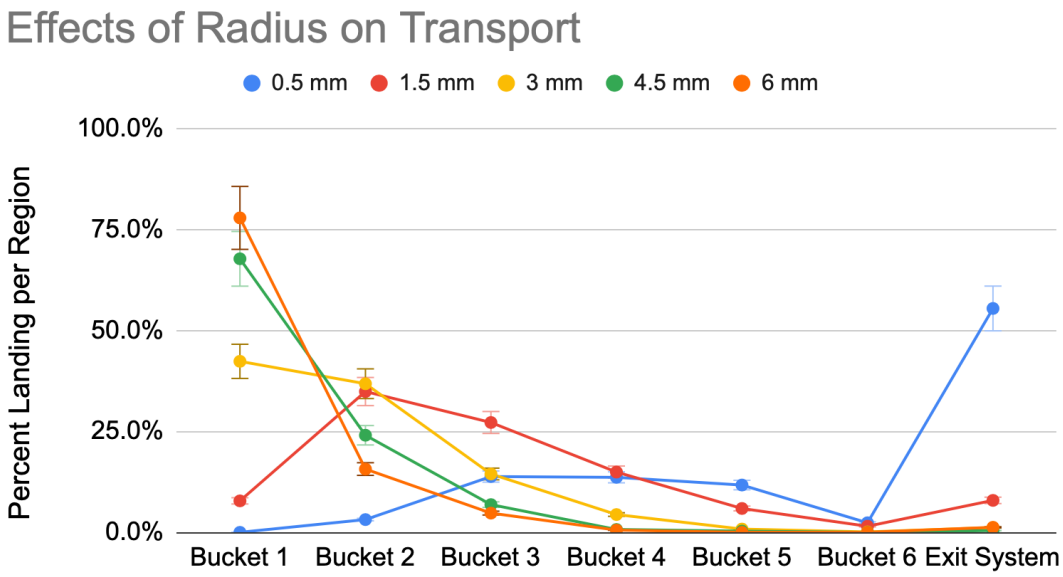

Figure A.8: Effects of Ember Radius on Transport (Course Trials)

The effects of ember density on ember transport for the additional course mesh trials are pictured below.

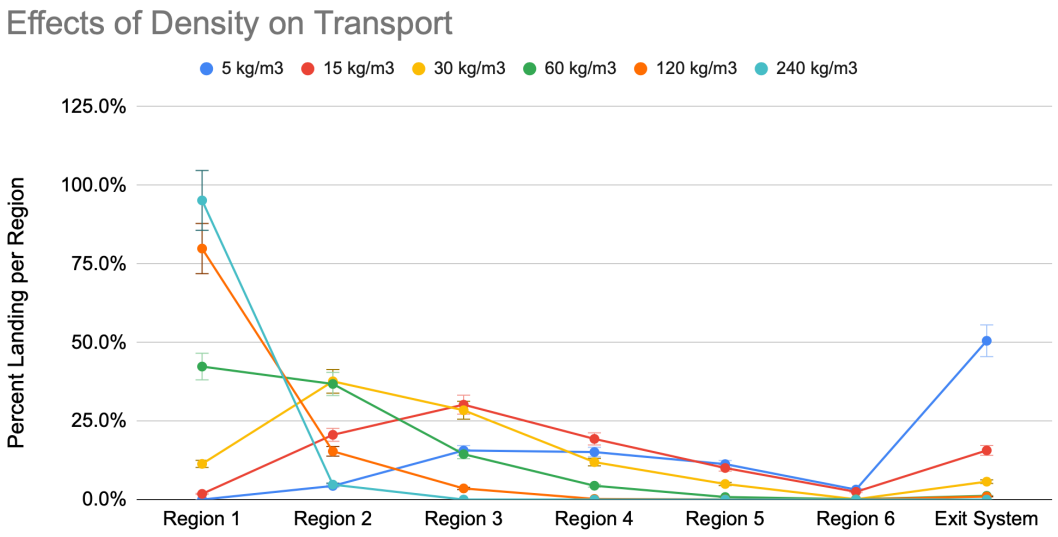

Figure A.9: Effects of Ember Density on Transport (Course Trials)

6.5. Effects of Wind Speed - Additional Trials

The effects of horizontal wind speed on ember transport for the additional course mesh trials are pictured below.

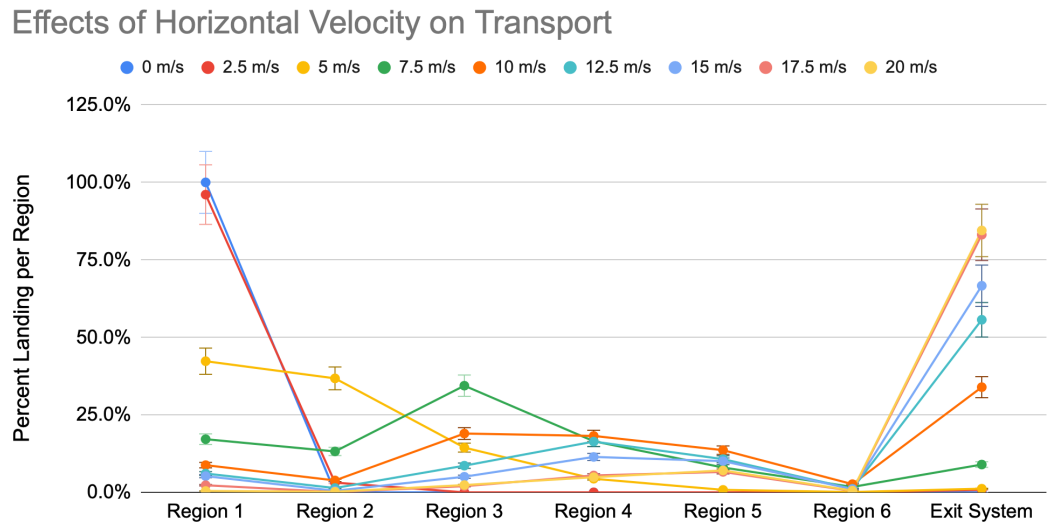

Figure A.10: Effects of Horizontal Wind Speed on Transport (Course Trials)

The effects of vertical wind speed on ember transport for the additional course mesh trials are pictured below.

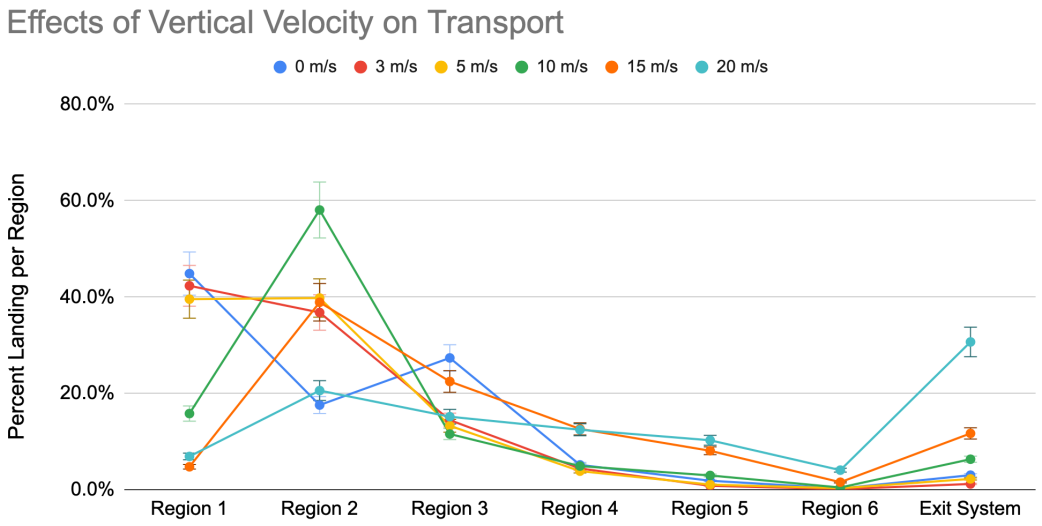

Figure A.10: Effects of Vertical Wind Speed on Transport (Course Trials)

6.6. Visualization of Ember Accumulation

Ember accumulation patterns and mass per unit volume concentrations for each trial of the building designs are pictured below.

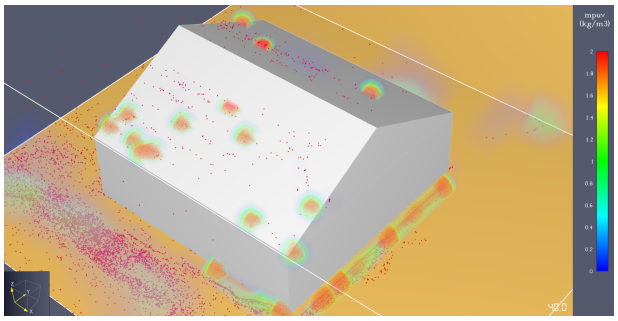

Figure A.11: Square Trial (0°)

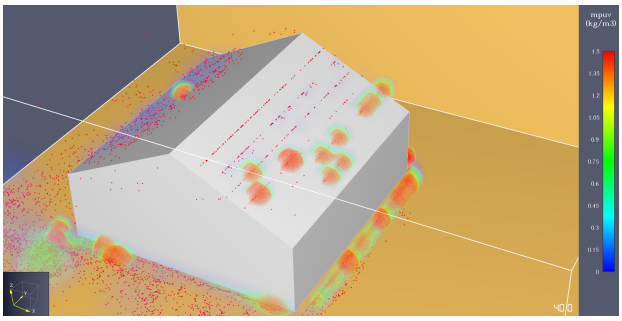

Figure A.12: Square Trial (90°)

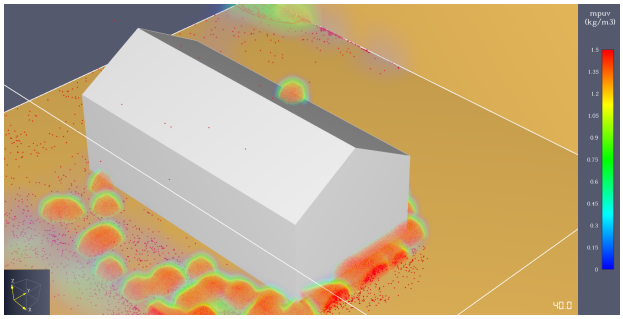

Figure A.13: Rectangular Trial (0°)

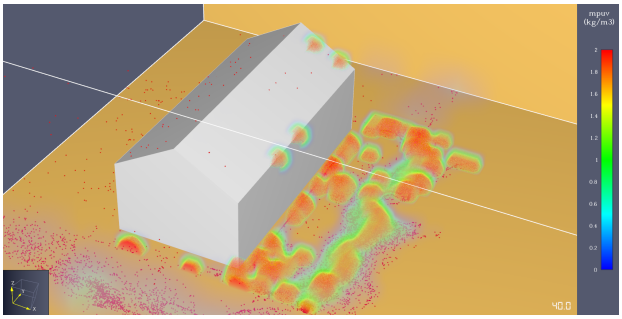

Figure A.14: Rectangular Trial (90°)

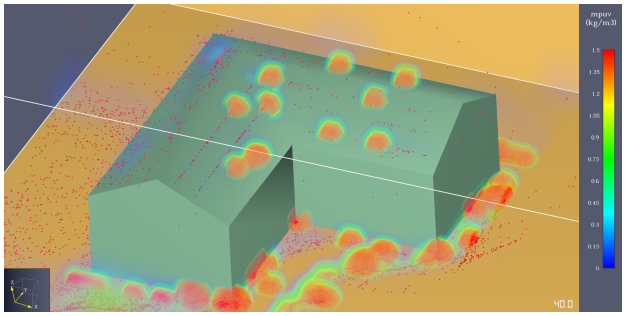

Figure A.15: L-Shape Trial (0°)

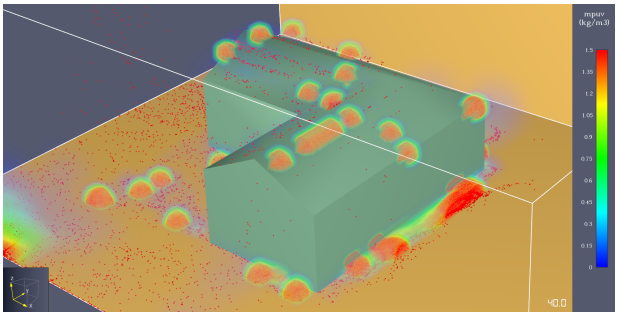

Figure A.16: L-Shape Trial (90°)

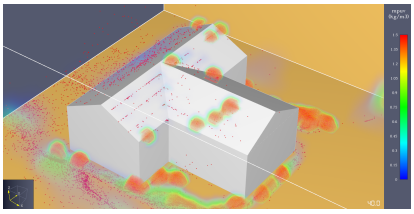

Figure A.17: T-Shape Trial (0°)

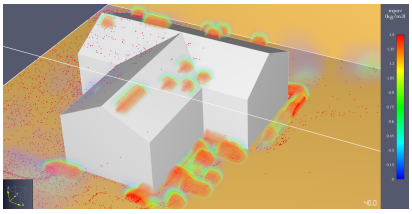

Figure A.18: T-Shape Trial (90°)

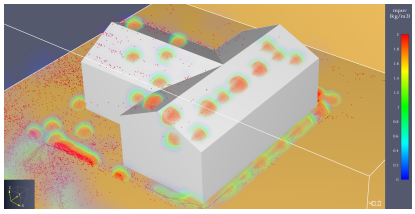

Figure A.19: T-Shape Trial (180°)

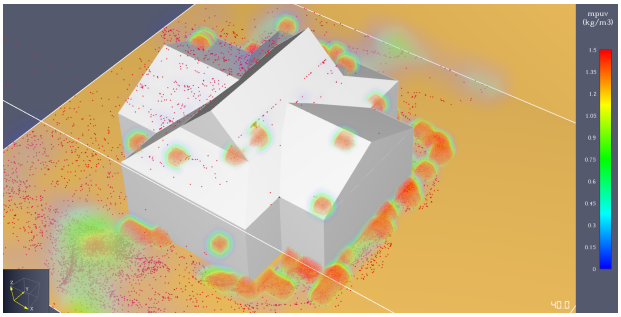

Figure A.20: IBHS Replica Trial (0°)

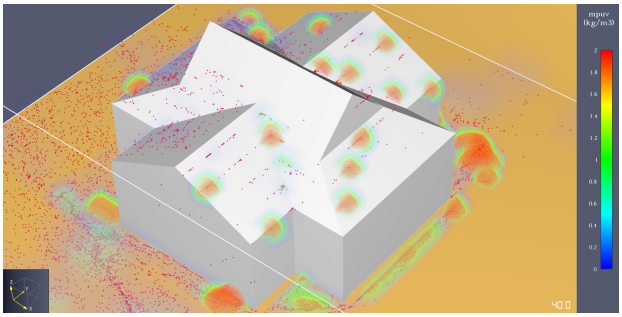

Figure A.21: IBHS Replica Trial (90°)

Ember accumulation patterns and mass per unit volume concentrations for each trial of the horizontal wind speed simulations are pictured below.

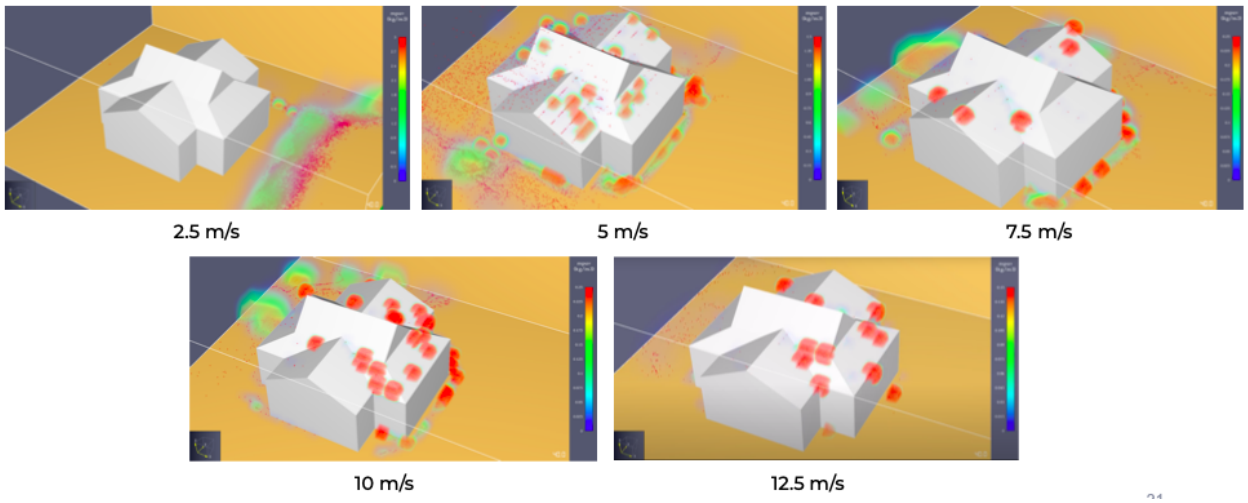

Figure A.22: IBHS Replica (90°) Horizontal Wind Speed Trials

6.7. Fire Effects on Benchmark Flow - Additional Plots

Below, we illustrate the velocity vector fields for the first case where a fire was introduced to the mock wind tunnel simulation. The orange plume denotes the location of the fire. For example, in the images portrayed, Case 1 implies that the fire was distance “h” ahead of the cube’s leading edge and placed at its center.

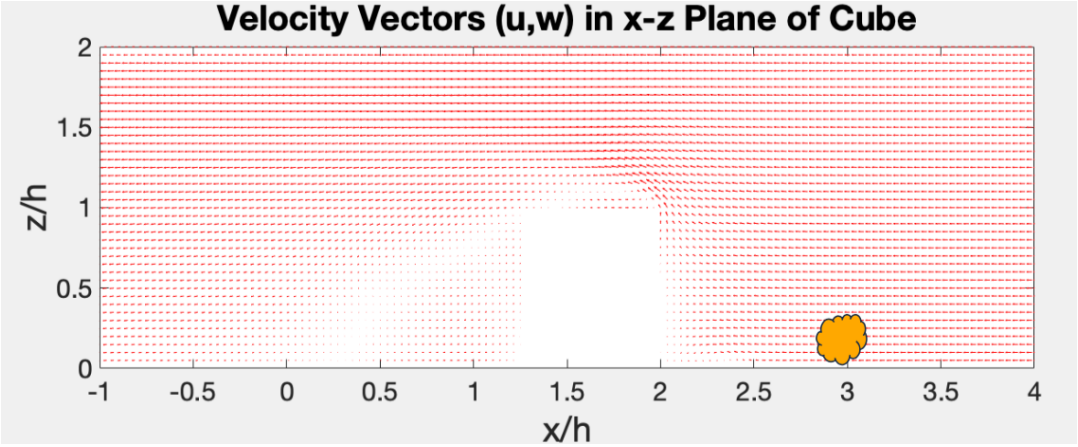

Figure A.23: Velocity Field in x-z Plane for Fire Case 1 (1000 W/m^2; Distance h)

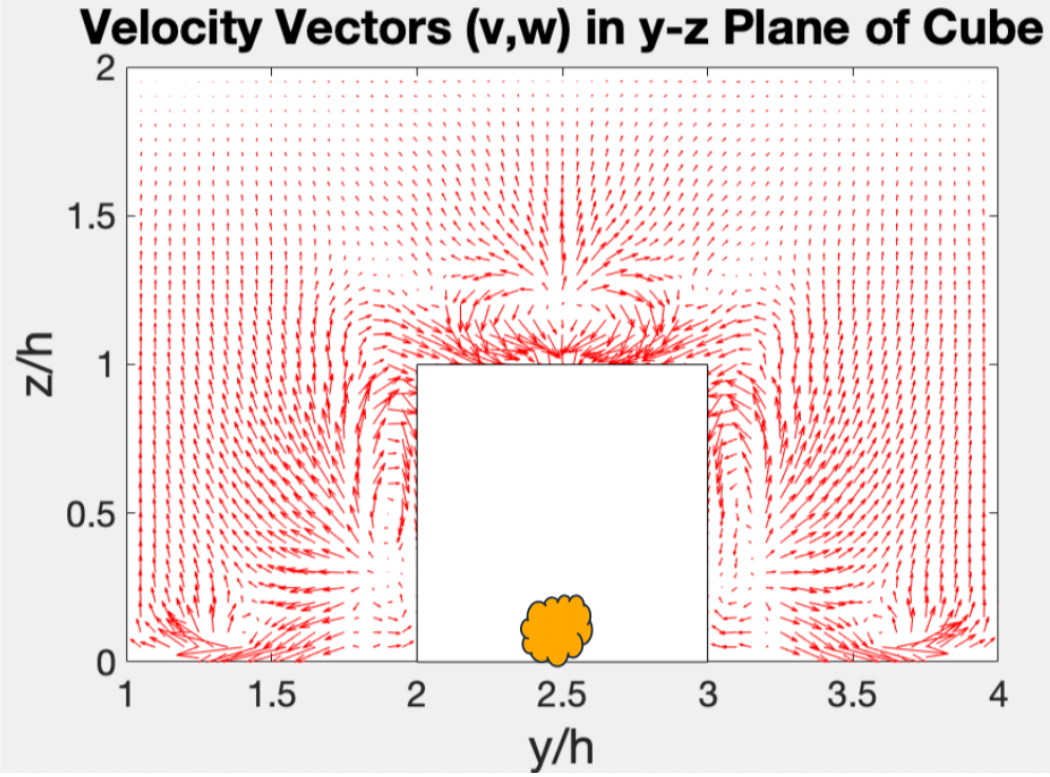

Figure A.23: Velocity Field in y-z Plane for Fire Case 1 (1000 W/m^2; Distance h)

Next, we provide the changes in mean vorticity for the two cases not provided in the main report. As noted in the main report, the fire-induced changes to vorticity do not differ significantly from the first test case.

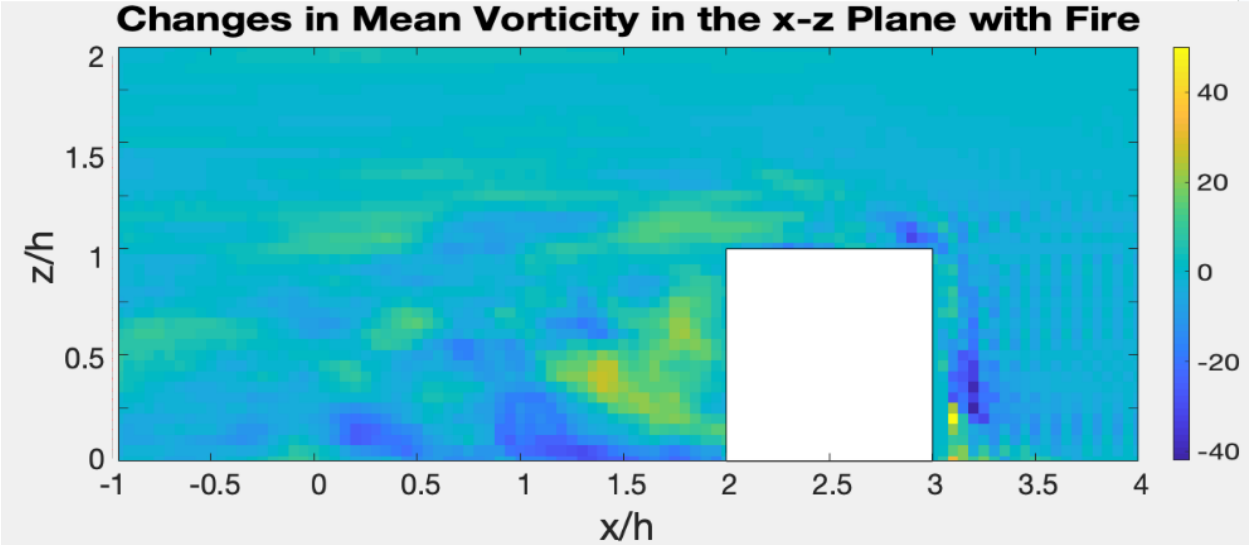

Figure A.24: Changes in Mean Vorticity (ω_y) Contour with Fire (3000 W/m^2; Distance h)

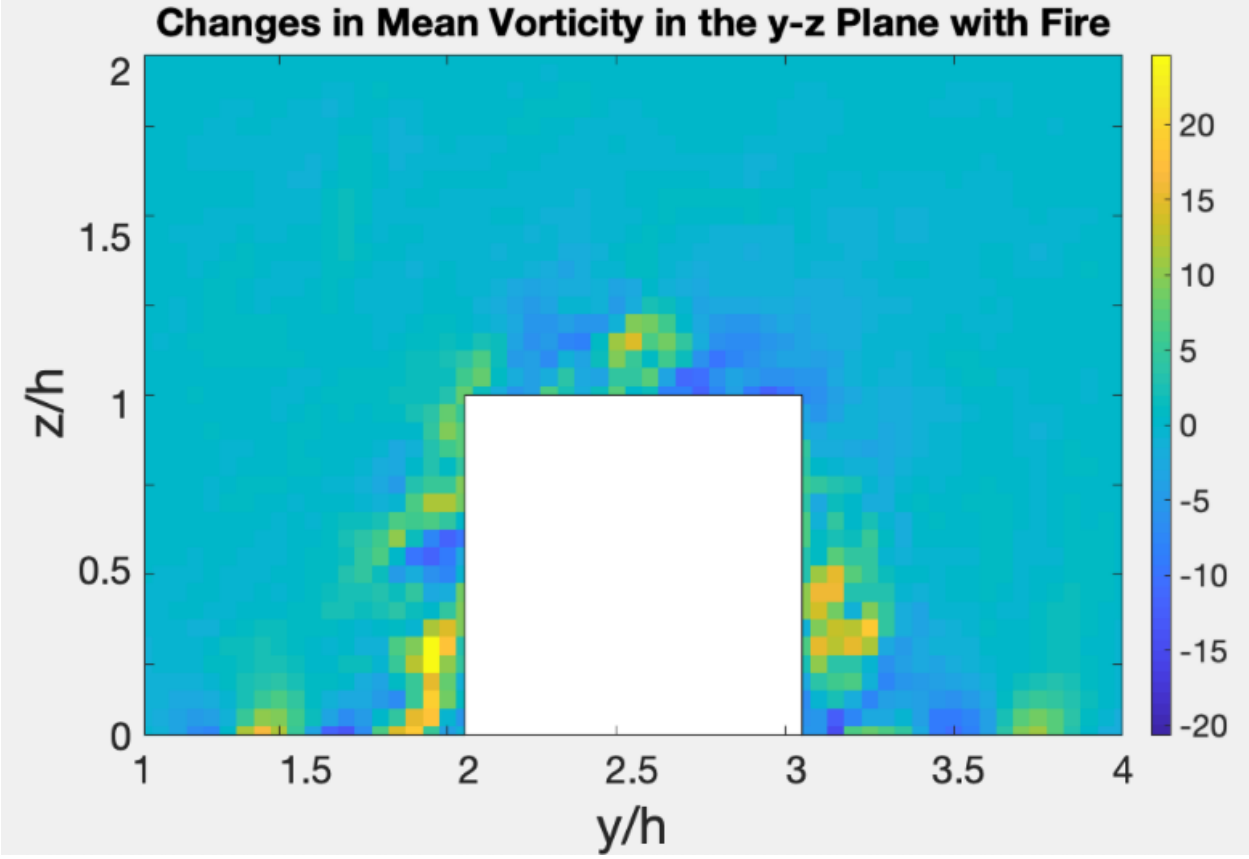

Figure A.25: Changes in Mean Vorticity (ω_x) Contour with Fire (3000 W/m^2; Distance h)

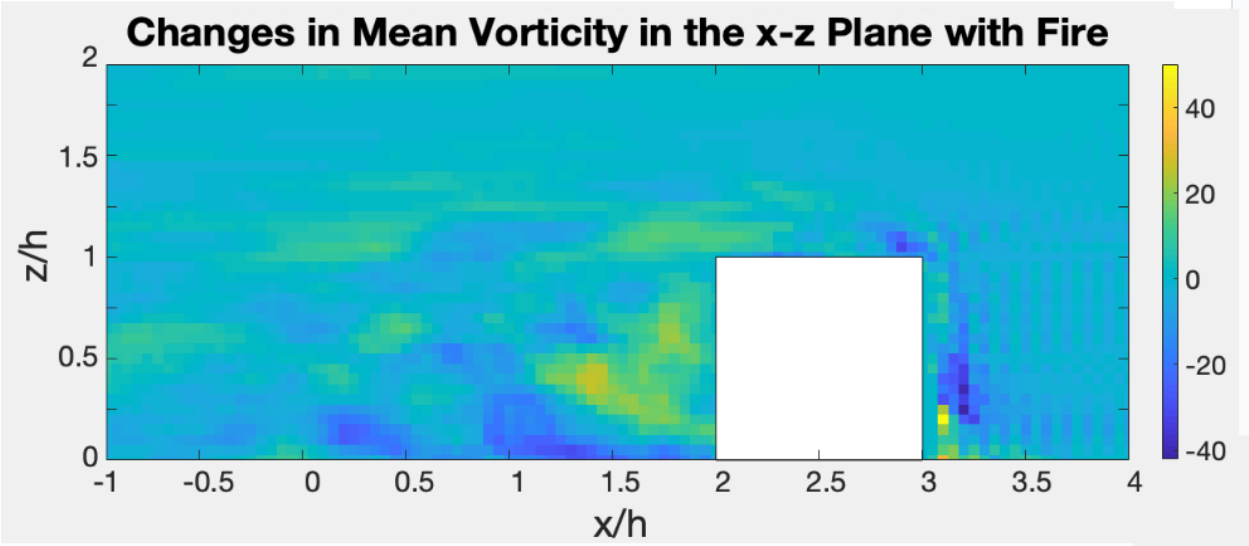

Figure A.26: Changes in Mean Vorticity (ω_y) Contour with Fire (1000 W/m^2; Distance h/2)

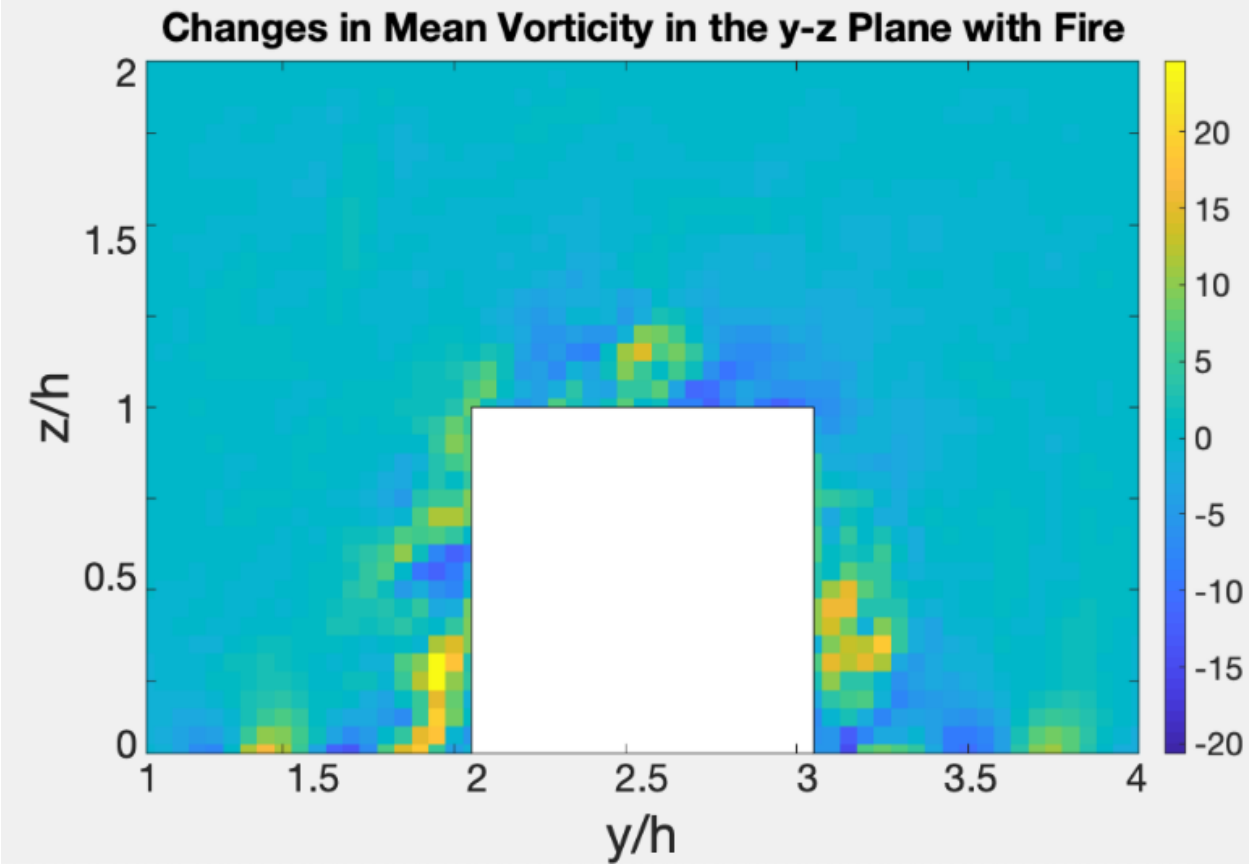

Figure A.27: Changes in Mean Vorticity (ω_x) Contour with Fire (1000 W/m^2; Distance h/2)